BOKU UNIVERSITY

Master Thesis

Monitoring Forest Loss in Tropical Dry Forests of Central Colombia: Global Datasets vs. Satellite Imagery

submitted by

Sabine SCHWEITZER, BSc

in the framework of the Master programme

Mountain Forestry

in partial fulfilment of the requirements for the academic degree

Master of Science

Vienna, July 2026

Supervisor

Dipl.-Ing. Dr. Markus Immitzer, M.Sc.
Institute of Geomatics
Department of Ecosystem Management, Climate and Biodiversity
Universität für Bodenkultur Wien

Co-supervisors

DDipl.-Ing. Michael Lechner, B.Sc.
Institute of Geomatics
Department of Ecosystem Management, Climate and Biodiversity
Universität für Bodenkultur Wien

Priv.-Doz. Dipl.-Ing. Dr. Andreas Melcher
Institute of Development Research
Department of Economics and Social Sciences
Universität für Bodenkultur Wien

Affidavit

I hereby declare that I have authored this master thesis independently, and that I have not used any assistance other than that which is permitted. The work contained herein is my own except where explicitly stated otherwise. All ideas taken in wording or in basic content from unpublished sources or from published literature, as well as those which were generated using artificial intelligence tools, are duly identified and cited, and the precise references included.

I further declare that this master thesis has not been submitted, in whole or in part, in the same or a similar form, to any other educational institution as part of the requirements for an academic degree.

I hereby confirm that I am familiar with the standards of Scientific Integrity and with the guidelines of Good Scientific Practice, and that this work fully complies with these standards and guidelines.

Vienna, 20.07.2026 Sabine SCHWEITZER *(manu propria)*

Preface

The research presented in this master thesis was conducted within the framework of the project *Las Mercedes "Reserva Natural de las Aguas": Accompanying Research CO_2 Compensation Colombia"*. It is coordinated by the Institute of Development Research (IDR) at BOKU University, with Priv.-Doz. Dipl.-Ing. Dr. Andreas Melcher is serving as project coordinator. The external cooperation partner is the Österreichisches Institut für Nachhaltige Entwicklung (ÖIN). Funding is provided by the BOKU Competence Centre for Climate Neutrality (*Kompetenzstelle für Klimaneutralität*) through its initiative *"Waldschutz im kolumbianischen Regenwald / Dorada"* (BOKU Kompetenzstelle für Klimaneutralität, 2026).

The accompanying research is embedded in the broader project *Las Mercedes – Reserva Natural de las Aguas*, which is coordinated by the ÖIN in close cooperation with the artists' association *ArtEmbassy*. This initiative combines scientific research, art, and carbon offsetting to promote forest conservation. It focuses on protecting forest ecosystems in central Colombia near La Dorada through model agriculture, conservation agreements with local communities, and research activities. Beyond ecological protection, the project aims to support sustainable regional development, create alternative income opportunities, and establish innovative research environments while fostering awareness for long-term ecological sustainability (BOKU Kompetenzstelle für Klimaneutralität, 2026; ÖIN, 2026).

Acknowledgements

I would like to express my sincere gratitude to my supervisor, Markus Immitzer, for his continuous support throughout the entire thesis process. His guidance, constructive feedback, and overall support during the development of this work were essential for its completion. I am also deeply grateful for his support during the fieldwork in Colombia and his help in shaping the methodological and conceptual framework of this study.

I would also like to thank my colleagues from the Institute of Geomatics. In particular, I am grateful to Michael Lechner for his assistance with R programming, and to Ardalan Daryaei for his support with PlanetScope imagery acquisition and cloud masking.

My sincere thanks go to Andreas Melcher for his coordination of the Las Mercedes project. I am equally grateful to Andreas Bauer for his help with drafting the abstract and for providing logistical support for the fieldwork in Colombia.

Special thanks go to Michael Stummer for his invaluable support during the fieldwork in Colombia, his expertise on water quality, and the many moments of productive collaboration and good humour in the field. I would also like to thank Ronny Miguel Quimbayo Garzón and Monica Astrauskas for their collaboration and support during field activities. Special thanks are also due to Carlos Devia from the Pontificia Universidad Javeriana for his expertise, time, and for enriching and highly interesting field excursions. Furthermore, I am grateful to the team at the Pontificia Universidad Javeriana in Bogotá, as well as the staff of the Las Mercedes Foundation, for their local expertise and logistical support.

I acknowledge the financial support provided by BOKU University, which made this research possible.

Finally, I would like to express my deepest gratitude to my family, friends, and my loving partner for their continuous emotional support, patience, and encouragement throughout my studies. Their support has been invaluable throughout this journey.

Table of content

Affidavit 1

Preface 2

Acknowledgements 3

Table of content 4

Abstract 6

Kurzfassung 7

1. Introduction 8

2. Material and Methods 11

2.1 Study Area 11

2.1.1 Location and Geography 11

2.1.2 Land Use and Vegetation: Tropical Dry Forests 12

2.2 Satellite Datasets 13

2.2.1 Planet Scope Imagery 13

2.2.2 Sentinel-2 Imagery 14

2.3 Forest mapping 15

2.3.1 Reference Points for Land Cover Classification 17

2.3.2 Land Cover Classification using Random Forest Models 19

2.3.3 Forest Cover Baseline Selection and Fragmentation Assessment 21

2.4 Forest Loss assessment 25

2.4.1 Change Detection based on Land Cover Classification 25

2.4.2 Change Detection based on Vegetation Index Thresholding using Reference areas 25

2.5 Global Forest Products 28

2.5.1 Hansen *et al.* Global Forest Change (GFC) 28

2.5.2 EC JRC Tropical Moist Forests (TMF) 28

3. Results 29

3.1 Land Cover Maps 29

3.2 Forest Cover Baseline 33

3.3 Forest Loss 36

4. Discussion 43

4.1 Evaluation of Land Cover Maps 43

4.2 Forest Cover Baseline Characterization 44

4.3 Comparison of Forest Loss Assessment Approaches 45

4.4 Forest Loss across Project Areas 46

4.5 Evaluation of Forest Loss Detection across Datasets: Comparison of Global Forest Products and Forest Loss Assessment 47

4.6 Conclusion 50

References 51

Declaration of the use of generative AI tools 56
List of figures 57
List of tables 59

Abstract

Tropical dry forests (TDF) are crucial for biodiversity, water regulation and carbon sequestration, but are increasingly threatened by agricultural expansion. Accurate forest loss monitoring is essential for their protection and sustainable management. In regions with restricted access due to terrain or security concerns, remote sensing plays a key role. Global forest datasets are widely used due to their accessibility, but their applicability for detecting forest loss in fragmented TDFs remains poorly understood. This thesis evaluates their suitability in Central Colombia by comparing them with a forest loss assessment based on high-resolution PlanetScope (PS) and Sentinel-2 (S2) imagery. Two global datasets are assessed: Global Forest Change (GFC) by Hansen et al. (2013) and EC JRC Tropical Moist Forest (TMF), both based on Landsat imagery. The analysis focuses on the Las Mercedes Reserve in the Upper Magdalena Valley, a fragmented landscape dominated by cattle ranching. Forest loss (2018–2024) was quantified using PS and S2 imagery through two complementary approaches: land cover (LC) classification and vegetation index (VI) change detection. Results show strong variation in detected forest loss across datasets due to sensor resolution and methodology. PS's 3 m resolution captures fine-scale disturbances, while S2 offers higher temporal and spectral consistency. LC approaches overestimate forest loss rates in the study area, particularly along edges, due to post-classification error propagation, with 28.96% (PS) and 29.42% (S2). VI methods yield more consistent estimates, with 5.34% (PS) and 2.58% (S2). GFC aligns well with VI results (1.84%), whereas TMF underestimates forest loss (0.18%), indicating limited suitability fragmented TDFs. Global datasets capture broad deforestation trends but require critical regional evaluation. Integrating them with high-resolution, site-specific data can improve forest monitoring in fragmented TDF systems.

Kurzfassung

Tropische Trockenwälder (TDFs) sind für Biodiversität, Wasserregulation und Kohlenstoffspeicherung von großer Bedeutung, stehen jedoch zunehmend unter Druck durch landwirtschaftliche Expansion. Ein präzises Monitoring von Waldverlusten ist entscheidend für ihren Schutz und eine nachhaltige Nutzung. In schwer zugänglichen Regionen aufgrund von Topografie oder Sicherheitslagen spielt Fernerkundung eine zentrale Rolle. Globale Walddatensätze werden häufig verwendet, ihre Eignung zur Erfassung von Waldverlust in fragmentierten TDFs ist jedoch bislang unzureichend untersucht. Diese Arbeit bewertet ihre Anwendbarkeit in Zentral-Kolumbien durch den Vergleich mit hochauflösenden PlanetScope- (PS) und Sentinel-2- (S2) Daten. Untersucht werden zwei globale Datensätze: Global Forest Change (GFC) nach Hansen et al. (2013) sowie EC JRC Tropical Moist Forest (TMF), beide basierend auf Landsat-Daten. Die Analyse konzentriert sich auf das Schutzgebiet Las Mercedes im oberen Magdalena-Tal, eine fragmentierte, von Rinderhaltung geprägte Landschaft. Der Waldverlust (2018–2024) wurde mithilfe von PS- und S2-Daten über zwei Ansätze bestimmt: Landbedeckungsklassifikation (LC) und Vegetationsindex-basierte (VI) Veränderungsanalyse. Die Ergebnisse zeigen deutliche Unterschiede aufgrund von Sensorauflösung und Methodik. PS (3 m) erfasst kleinräumige Störungen, während S2 eine höhere zeitliche und spektrale Konsistenz bietet. LC-Ansätze überschätzen den Waldverlust, insbesondere an Rändern, infolge von Fehlerfortpflanzung (28,96% PS; 29,42% S2). VI-Methoden liefern konsistentere Werte (5,34% PS; 2,58% S2). GFC stimmt gut mit VI-Ergebnissen überein (1,84%), während TMF den Waldverlust unterschätzt (0,18%) und nur eingeschränkt für TDFs geeignet ist. Globale Datensätze erfassen großräumige Trends, ihre regionale Anwendbarkeit sollte jedoch kritisch geprüft werden. Die Kombination mit hochauflösenden, standortspezifischen Daten verbessert das Monitoring in fragmentierten TDFs.

1. Introduction

Tropical forests provide essential ecosystem functions that regulate life on Earth, including global biogeochemical cycles, carbon sequestration, and climate regulation (Harris *et al.*, 2018; Watson *et al.*, 2018; Vancutsem *et al.*, 2021). Globally, tropical forests are typically classified as tropical rain forest, moist tropical forest, and dry tropical forest (Murphy and Lugo, 1986).

Among these, tropical dry forests (TDFs) are variable ecosystems, and definitions differ across studies (Murphy and Lugo, 1986). They are generally characterized by pronounced seasonality, with prolonged dry periods lasting between three and nine months and annual precipitation ranging from 250 to 2,000 mm (DRYFLOR et al., 2016; Hasnat & Hossain, 2020; Pérez-Escobar et al., 2022).

A main ecological feature of these forests is the deciduous leaf phenology of many woody species, which is driven by water deficits during the dry seasons (Bullock et al., 1995; Dirzo et al., 2011; Murphy & Lugo, 1986; Portillo-Quintero & Sánchez-Azofeifa, 2010). TDFs can be distinguished as a unique biome (Dexter *et al.*, 2018). The vegetation ranges from tall forests in moister areas to cactus scrub in the driest sites, with a high degree of ecological specialization (DRYFLOR *et al.*, 2016; González-M *et al.*, 2018; Pérez-Escobar *et al.*, 2022). Approximately 40% of woody plant species in TDFs are endemic (Hasnat and Hossain, 2020). Studies report high species turnover across and within regions of TDFs in Latin America (Linares-Palomino, Oliveira-Filho and Pennington, 2011; DRYFLOR *et al.*, 2016), along with high regional endemism (González-M *et al.*, 2018).

Globally, TDFs cover approximately 42% of tropical and subtropical forest area and occur across five of the eight global biogeographic realms, including the Americas, Africa, Eurasia, Australia, and Southeast Asia (Hasnat and Hossain, 2020). Janzen (1988) describes TDFs as the most endangered major tropical ecosystem. Although these forests have a wide potential distribution (Olson *et al.*, 2001), less than 10% of their original extent remains in several countries (Miles *et al.*, 2006; Portillo-Quintero and Sánchez-Azofeifa, 2010; Pizano and García, 2014) and they are poorly represented in protected areas (DRYFLOR *et al.*, 2016; González-M *et al.*, 2018). Globally, 97% of remaining TDFs are at risk from one or more anthropogenic threats, including climate change, habitat fragmentation, fire, high human population density, and conversion to cropland (Miles *et al.*, 2006), as illustrated in Figure 1.

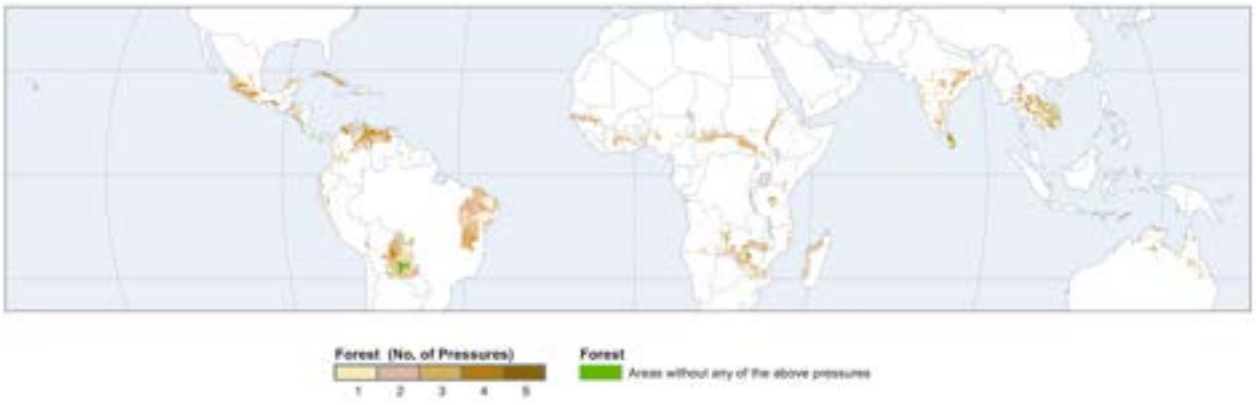


Figure 1: Global distribution of tropical dry forest illustrating spatial variation in exposure to threats, including climate change, habitat fragmentation, fire, population density, and cropland conversion. The map shows tropical dry forest extent in 2000 based on biogeographic realms (Olson *et al.*, 2001) and MODIS 500 m forest cover data, with canopy cover > 40% (Hansen *et al.*, 2003). Robinson projection. Source: Miles et al. (2006).

TDFs frequently occur on fertile soils in climates favourable to human settlement, which has made them highly attractive for agricultural expansion. Compared to tropical rainforests, they are easier to clear and better suited for crop production and livestock grazing, leading to their widespread conversion and role as early frontiers of economic development (Murphy and Lugo, 1986; Dirzo *et al.*, 2011; Hasnat and Hossain, 2020).

More than half (54.2%) of the remaining TDFs are located within South America (Miles et al., 2006). Within the Americas, Colombia contains 6.5% of the total TDF area, but 67% of the potential TDF cover in the country has already been converted to other land uses (Olson *et al.*, 2001; Portillo-Quintero and Sánchez-Azofeifa, 2010). The actual extent of forest cover in the Colombian TDF life zone is largely unknown, especially in heterogeneous landscapes dominated by an agricultural matrix (Fernández-Méndez *et al.*, 2013).

The Colombian Andes consist of three mountain ranges separated by two large intra-mountain valleys, the Cauca and Magdalena River valleys. This high topographic and climatic variability generates mosaics of moist and dry forest over short distances (Fernández-Méndez *et al.*, 2013; Pizano and García, 2014; DRYFLOR *et al.*, 2016; González-M *et al.*, 2018; Pérez-Escobar *et al.*, 2022). Historically, the Magdalena River Valley has experienced extensive agricultural and infrastructure development, resulting in forest loss (Fernández-Méndez *et al.*, 2013; González-M *et al.*, 2018). In the department of Caldas, an estimated 91% of the potential TDF cover has been converted to other land uses (Fagua and Jantz, 2024).

Within the inter-Andean valleys of Colombia, remaining TDFs fragments persist mainly on steep slopes and along riparian corridors, where they occur as small, irregular patches (Fernández-Méndez *et al.*, 2013; Pizano and García, 2014; González-M *et al.*, 2018). A nationwide field survey found that most remnants are in early or intermediate successional stages, with little mature forest remaining. Most common tree species were generalists that are favoured by forest disturbance (González-M *et al.*, 2018). These conditions reduce ecological integrity and increase vulnerability to further degradation, particularly in secondary forests (Bianchi & Haig, 2013; Sánchez-Azofeifa *et al.*, 2013).

Within this context, this thesis focuses on the “Las Mercedes – Reserva Natural de las Aguas”, located in the Magdalena River valley in central Colombia. The reserve represents a fragmented TDF containing a mosaic of primary forest, secondary regrowth, and human-influenced areas. The project integrates conservation, climate protection, and cultural initiatives, in collaboration with ÖIN, BOKU University Vienna, ArtEmbassy, and Javeriana University Bogotá (BOKU Kompetenzstelle für Klimaneutralität, 2026; ÖIN, 2026).

Accurately identifying where TDFs persist and how they change over time has become a central challenge for conservation and land management due to their extensive loss and fragmentation (Fernández-Méndez *et al.*, 2013; Hesketh and Sánchez-Azofeifa, 2014; Gyamfi-Ampadu and Gebreslasie, 2021). This challenge is particularly evident in the inter-Andean valleys of Colombia, including the Magdalena River Valley, where spatially explicit information on forest extent and condition remains limited and dry forests occur as highly heterogeneous mosaics embedded within agricultural landscapes (Fernández-Méndez *et al.*, 2013; Fagua and Jantz, 2024). Fragmentation, small patch size, and pronounced edge effects complicate the detection and monitoring of forest remnants. As a result, current knowledge of forest distribution and landscape dynamics remains incomplete, constraining conservation planning and ecosystem management (Sánchez-Azofeifa *et al.*, 2013; Hasnat and Hossain, 2020). Reliable estimates of TDF cover and distribution are therefore essential not only for conservation planning but also as part of broader land use and land cover assessments (Galiatsatos *et al.*, 2020; Ferrer Velasco *et al.*, 2022). However, existing maps frequently overestimate tropical moist forests while underestimating TDFs, limiting the reliability of regional assessments and associated ecological indicators (Portillo-Quintero & Sánchez-Azofeifa, 2010).

Accurate mapping of TDFs increasingly relies on remote sensing. Earth Observation data complement ground-based inventories by providing consistent, repeatable measurements of forest extent and change across large and often inaccessible regions (Da Ponte *et al.*, 2015; Gyamfi-Ampadu and Gebreslasie, 2021). Satellite imagery enables frequent temporal monitoring, capturing seasonal and phenological dynamics that influence vegetation structure and detectability (Hesketh and Sánchez-Azofeifa, 2014). These observations have enhanced the understanding of forest degradation, spatial patterns, and ecosystem responses to climatic variability (Fernández-Méndez *et al.*, 2013).

Remote sensing also offers a low-cost and widely accessible source of information for national and regional reporting (Ferrer Velasco *et al.*, 2022). Over the past decades, a variety of global and regional forest cover datasets have been developed using satellite imagery at different resolutions and classification approaches (Galiatsatos *et al.*, 2020; Ferrer Velasco *et al.*, 2022). Miles et al. (2006) combined MODIS Vegetation Continuous Fields (VCF) data, depicting percentage tree cover at 500 m resolution, with biome classifications to produce a global distribution map of TDFs (Figure 1). Similarly, Portillo-Quintero and Sánchez-Azofeifa (2010) used MODIS surface reflectance imagery at 500 m to assess the extent of Neotropical dry forests. At 30m resolution, Landsat imagery has played a central role in forest mapping and change detection analysis by offering long-term, continuous, and freely available global data (Hansen *et al.*, 2013; Gyamfi-Ampadu and Gebreslasie, 2021). Availability, quantity, and quality of forest cover and land-use datasets have improved substantially in recent decades (Galiatsatos *et al.*, 2020; Ferrer Velasco *et al.*, 2022).

Two widely used global forest datasets are analysed in this thesis. The Hansen et al. (2013) Global Forest Change (GFC) dataset provides annual forest cover and loss estimates, based on Landsat and enables consistent large-scale monitoring of deforestation dynamics. Across REDD+ countries, GFC has been shown to provide a cost-effective and comparable proxy for tropical deforestation (Harris *et al.*, 2018). The European Commission Joint Research Centre (EC JRC) Tropical Moist Forest (TMF) dataset offers annually updated, peer-reviewed maps of tropical forest extent and change derived from Landsat time series (Vancutsem *et al.*, 2021). While these products support standardized temporal analyses, their coarse resolution may miss small, fragmented forest patches.

Higher-resolution satellite imagery can help address this limitation. For instance, Sentinel-2 (S2) and RapidEye, now provide sufficiently long archives for multi-temporal forest monitoring, as suggested by (Gyamfi-Ampadu and Gebreslasie, 2021). In Colombia, Fagua and Jantz (2024) mapped TDFs using S2 (10 m) and found substantially greater forest extent than national Landsat-based maps, highlighting the importance of spatial resolution. Comparative studies in Morocco also show that PlanetScope (PS) imagery (3 m) can outperform Landsat and S2 in detailed land cover (LC) mapping (Acharki, 2022).

Building on these insights, this thesis evaluates the performance of global forest monitoring products in a fragmented TDF landscape in the Magdalena River Valley, focusing on the “Las Mercedes – Reserva Natural de las Aguas”.

It addresses the following research questions:

1. To what extent can higher-resolution satellite imagery (S2 and PS) provide more detailed and accurate information on forest cover and forest loss compared to global forest datasets?
2. How well do global forest monitoring products (GFC and TMF) represent forest cover and forest loss in fragmented TDF landscapes in the study area?

To answer these questions, high-resolution LC maps are generated for the study area for the period 2018 – 2024 using S2 and PS imagery. The baseline forest structure and fragmentation in 2018 are then characterized, followed by an assessment of annual forest loss using two complementary approaches: change detection based on LC classification and vegetation index (VI) thresholds. The resulting estimates are compared with the GFC and TMF datasets to evaluate their performance in a fragmented TDF context.

It is expected that global datasets capture broad deforestation trends but underestimate forest loss in small, spatially heterogeneous patches. Integrating global and high-resolution datasets may therefore improve monitoring accuracy and support conservation and land-management decisions.

2. Material and Methods

2.1 Study Area

2.1.1 Location and Geography

The study area is located in central Colombia, approximately between Bogotá and Medellín in the Upper Magdalena River Valley. The Magdalena River, Colombia's largest river, flows northward through the Andes to the Caribbean Sea, dividing the Central Mountain range (Cordillera Central) and the Western Mountain range (Cordillera Oriental) of the Andes.

In total, the Colombian Andes consist of three mountain ranges (Eastern, Central, and Western) separated by two intra-mountain valleys, the Cauca and Magdalena River valleys (Gregory-Wodzicki, 2000). Elevation ranges from ~50 to 5,300 m, creating steep climatic gradients and a mosaic of tropical dry forests and tropical moist forests over short distances (Pizano and García, 2014).

The Andes region, Colombia's most densely populated region, has undergone extensive conversion of natural forests to anthropogenic land uses, including crops, pastures, plantations, and infrastructure (Etter, McAlpine and Possingham, 2008; Armenteras *et al.*, 2011). While much of the forest is now fragmented, some large, continuous areas remain, especially on the western slope of the Western Mountain range and the eastern slope of the Eastern Mountain range (Hansen *et al.*, 2013).

For this study, a broader Area of Interest (AOI) was defined to include the three project areas of the "Reserva Natural de las Aguas", Las Mercedes, La Roka, and El Triunfo, as well as the Purnio River and nearby sections of the Magdalena River (Figure 2). It spans parts of the departments of Tolima, Caldas, and Cundinamarca. The major cities within the AOI are Mariquita, Honda, and La Dorada. The AOI covers approximately 216,115 ha, ranging from 160 to 1,465 m above sea level (masl), located at roughly 5° N and -75° W (WGS 84).

The three project areas of "Reserva Natural de las Aguas" are:

- **Las Mercedes** (535 ha): Northern AOI, with partially untouched vegetation around Loma de Yarumal (731 masl). The climate is relatively moist.
- **La Roka** (740 ha): South of Las Mercedes, adjacent to the Guarino River, at 250–400 masl. The climate is comparatively dry.
- **El Triunfo** (7,277 ha): South of Honda, at 250–800 masl, characterized by a dry climate.

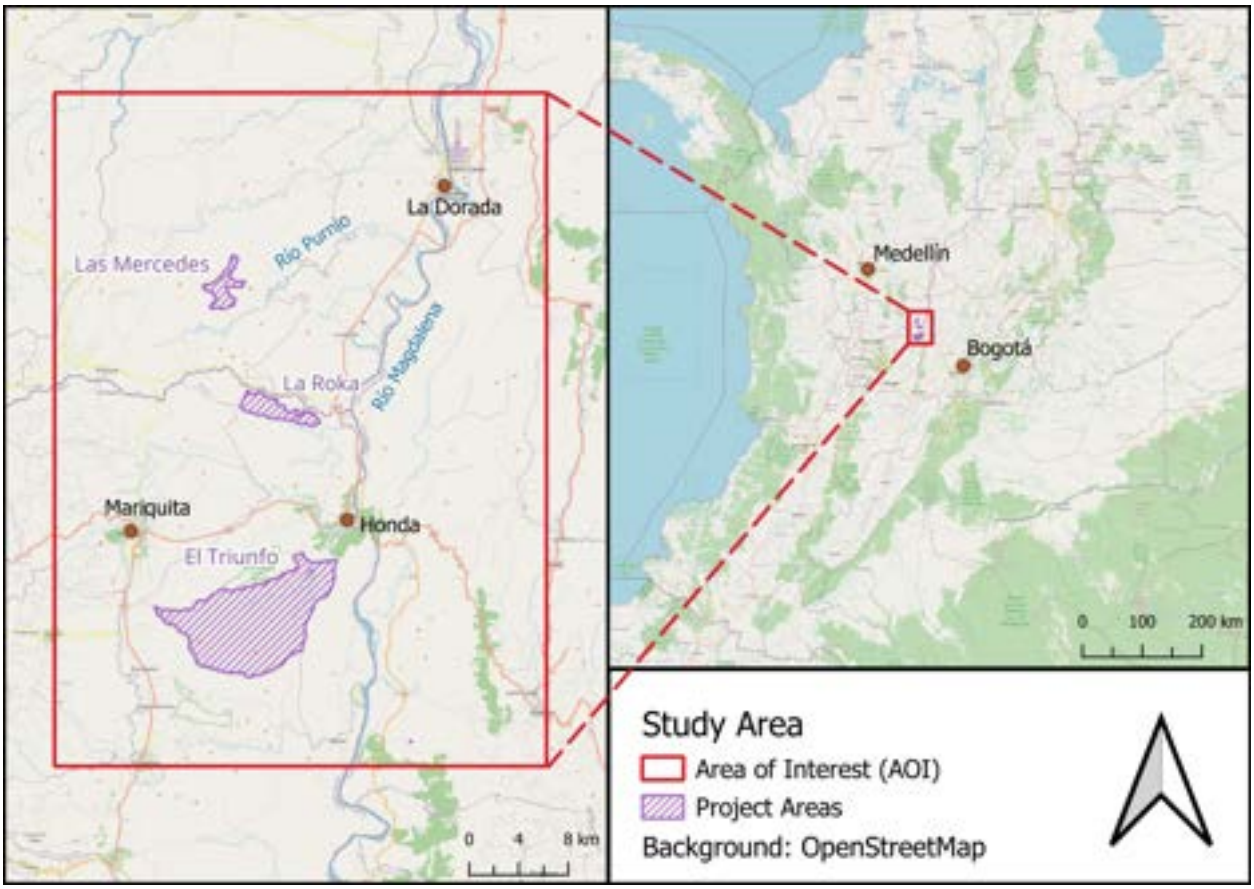


Figure 2: Study Area in Central Colombia. Area of Interest (AOI) in red and the project areas of the "Reserva Natural de las Aguas" (Las Mercedes, La Roka, and El Triunfo) in purple. Cities are marked as brown points.

2.1.2 Land Use and Vegetation: Tropical Dry Forests

The AOI is dominated by tropical dry forests (TDFs), part of the Neotropical realm and the tropical and subtropical dry broadleaf forests biome (Hasnat and Hossain, 2020). These ecosystems are critically endangered and are considered one of the most threatened forest types (Janzen, 1988; Miles *et al.*, 2006; Portillo-Quintero and Sánchez-Azofeifa, 2010; Fernández-Méndez *et al.*, 2013).

Definitions of TDFs vary with rainfall, dry season length, temperature, and evapotranspiration (Murphy and Lugo, 1986; Bullock, Mooney and Medina, 1995; Portillo-Quintero and Sánchez-Azofeifa, 2010; Dirzo *et al.*, 2011). Despite this variability, they are consistently characterized by deciduous tree species, with leaf shedding driven by water deficits during dry seasons (Bullock, Mooney and Medina, 1995; Portillo-Quintero and Sánchez-Azofeifa, 2010; Dirzo *et al.*, 2011; Dexter *et al.*, 2018).

The Magdalena Valley represents a prime example of Andean TDFs in Colombia (Pizano and García, 2014; González-M *et al.*, 2018). Historically, the valley has undergone extensive transformation due to the intensification of agriculture and infrastructure development (Etter, McAlpine and Possingham, 2008). In the department of Caldas, fertile soils have promoted intensive land use, leading to substantial deforestation (Portillo-Quintero and Sánchez-Azofeifa, 2010; Fagua and Jantz, 2024). Despite these pressures, some continuous forest patches remain. Today, the landscape is a dynamic mosaic of primary TDF, secondary regrowth, and agricultural areas (Miles *et al.*, 2006; Sánchez-Azofeifa *et al.*, 2013; González-M *et al.*, 2018; IDEAM, PNN and Sinchi, 2021). Figure 3 illustrates a typical landscape scenario.

TDFs in Colombia remain largely understudied regarding ecosystem functionality (Fernández-Méndez *et al.*, 2013). Information on species composition, forest cover, and conservation status is limited, and few monitoring programs exist to guide protective measures (Sánchez-Azofeifa *et al.*, 2013; Hasnat and Hossain, 2020). These forests play a critical role in maintaining local biodiversity and regulating water cycles but remain highly fragmented and threatened by human activity (Portillo-Quintero and Sánchez-Azofeifa, 2010; Pizano and García, 2014; DRYFLOR *et al.*, 2016).



Figure 3: Pasture and forest patches in the project area El Triunfo, Colombia, August 2024. Image: author's own.

2.2 Satellite Datasets

2.2.1 Planet Scope Imagery

PlanetScope is a satellite constellation operated by Planet Labs (Planet Labs PBC, 2025), consisting of more than 150 CubeSats ("Doves") in near-polar orbit at an altitude of approximately 475 km. The constellation has been continuously recording data since 2016 and has expanded through successive Dove generations with enhanced sensor systems. Current PS imagery provides a spatial resolution of 3 m, a daily revisit time, eight spectral bands, and is available commercially (Planet Labs PBC, 2025).

PS imagery from 2018 to 2024 was analysed. The year 2018 was selected as the starting point to ensure consistent image availability from both PS and S2.

To minimize seasonal variation, only scenes from July to September with cloud-free or nearly cloud-free conditions were selected for each year.

Due to incomplete AOI coverage within a single scene, mosaics were generated. For each year, the largest and most suitable scene was selected as the primary image, and the remaining gaps were filled with one to two additional scenes. A visual quality assessment was performed to exclude images with spectral distortions, such as rainbow artifacts or exaggerated colour tones. As a result, the resulting mosaics were not fully homogeneous, and minor cloud cover remained in some cases.

From 2018 to 2021, PS provided four spectral bands: blue, green, red, and near-infrared (NIR). For 2022 – 2024, data were available in eight bands: coastal blue, blue, green I, green, yellow, red, red edge, NIR (Planet Labs PBC, 2025). For each year, the selected spectral bands were combined into a multi-layer stack for further analysis. Raster data preprocessing, mosaicking and layer stack creation were carried out using the *terra* package in R (R Core Team, 2021; Hijmans, 2025).

2.2.2 Sentinel-2 Imagery

The Copernicus S2 mission consists of two identical satellites in the same orbit, each equipped with a multispectral instrument capturing 13 spectral bands at spatial resolutions of 10 m, 20 m, or 60 m, depending on the band. S2A was launched on 23 June 2015 and S2B on 7 March 2017, providing a combined revisit time of five days. In 2025, S2A was replaced by S2C (ESA, 2025). Data are freely available for visualization and download via the Copernicus Data Space Ecosystem (Copernicus, 2025).

S2 imagery from 2018 to 2024 was analysed, with 2018 selected as the starting point to ensure consistency with PS data availability. To minimize seasonal variation, scenes from July to September were selected, aiming for cloud-free or nearly cloud-free conditions each year. However, fully cloud-free scenes could not be obtained due to the generally high cloud cover in the AOI.

Automated cloud-masking approaches were tested, including the S2 Scene Classification Layer (SCL) (ESA, 2025) and composite generation in Google Earth Engine (Google Earth Engine, 2025). These methods produced unsatisfactory results, as clouds and shadows remained visible, and composites were inhomogeneous with missing pixel values. Therefore, two to three partially cloud-covered scenes were selected per year. Individual cloud mask layers were created manually in QGIS (QGIS.org, 2025) and the largest and most suitable scene was selected as the primary image. Clouded areas were filled with one or two additional scenes. As a result, the mosaics were not fully homogeneous, and minor cloud cover remained.

Level-2A products with atmospheric correction were used (ESA, 2025). Since the AOI spans two tiles, both tiles were cropped to the AOI, and differences in atmospheric correction were adjusted by applying a linear regression model to the northern tile based on its overlap with the southern tile.

The six S2 bands originally acquired at 20 m resolution were resampled to 10 m using the nearest-neighbour method (Hijmans, 2025). A final layer stack was generated, including the ten spectral bands: B2, B3, B4, B5, B6, B7, B8, B8A, B11 and B12. All raster preprocessing, mosaicking and layer stack creation were performed in R using the *terra* package (R Core Team, 2021; Hijmans, 2025).

2.3 Forest mapping

The overall workflow of the forest mapping and forest loss assessment is illustrated in Figure 4. The workflow is structured into three main components: (1) forest cover mapping, (2) forest loss assessment, and (3) comparison with global forest datasets.

In the first step, pre-processed satellite imagery served as the basis for forest mapping through supervised LC classification. This step resulted in a high-resolution forest cover baseline for the year 2018 based on PS imagery.

In the second step, forest loss was assessed using two complementary approaches applied to both PS and S2 imagery. The first approach identifies forest loss based on annual LC classifications, while the second approach detects changes in VIs over time. To ensure consistency, non-forest areas were masked using the 2018 Forest Cover Baseline. This process resulted in four forest loss products derived from the combination of sensors and methods.

In the final step, global forest datasets were integrated and adapted to the spatial extent and temporal range of the study area. These include the GFC and the TMF dataset. The global products were then compared with the locally derived forest loss maps to evaluate their suitability for monitoring fragmented TDFs.

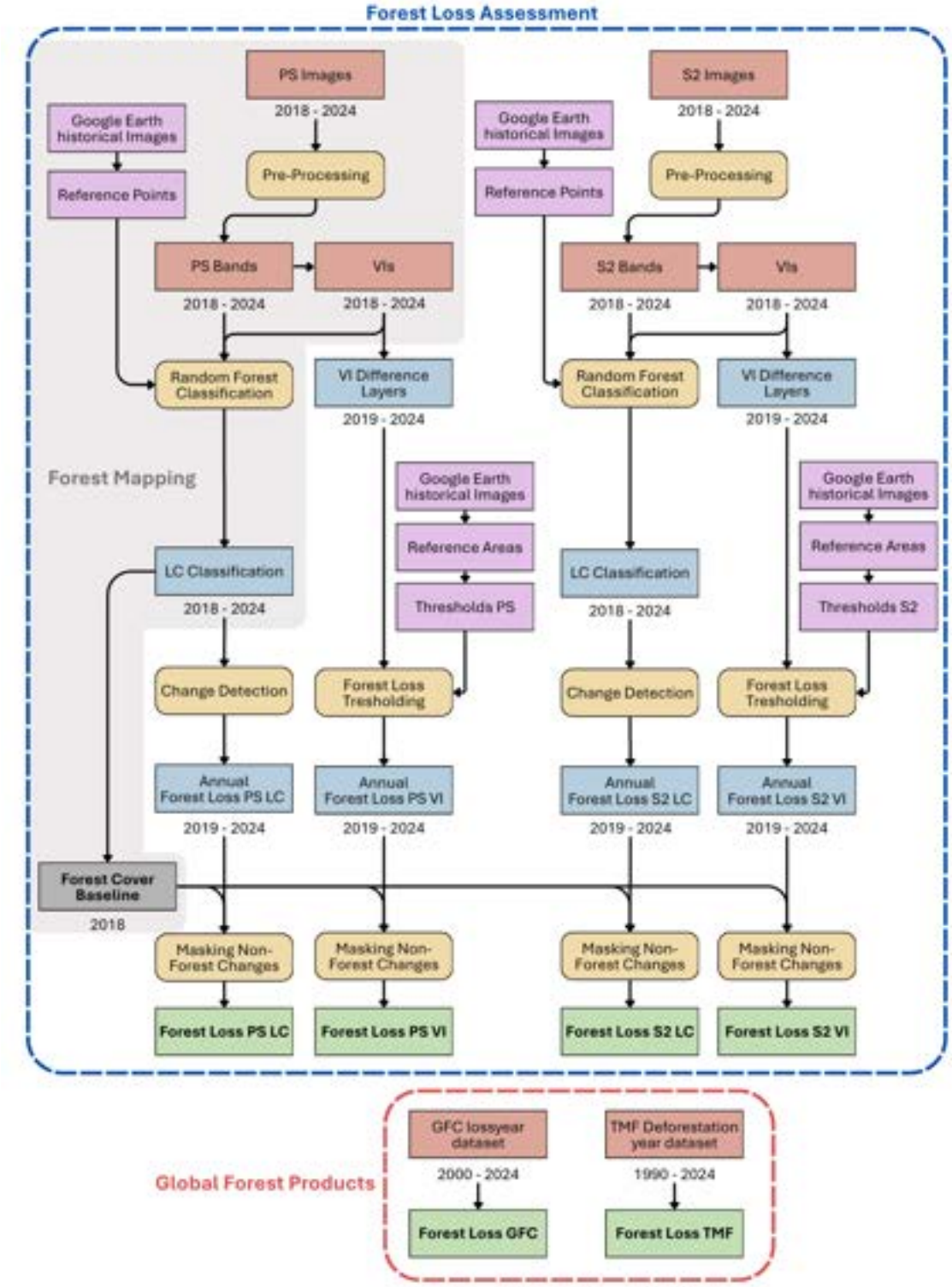


Figure 4: Flowchart illustrating the workflow of forest cover mapping and forest loss assessment. Rectangles represent data inputs and outputs, while rounded shapes indicate processing steps. Colours distinguish data types: red = input data, purple = auxiliary/reference data, blue = intermediate products, and green = final outputs. The workflow is divided into three components: forest cover mapping (grey background), forest loss assessment (blue dashed frame), and comparison with global forest products (red dashed frame). Abbreviations: PS = PlanetScope; S2 = Sentinel-2; VI = vegetation index; LC = land cover; GFC = Global Forest Change; TMF = Tropical Moist Forest.

2.3.1 Reference Points for Land Cover Classification

Four LC classes were defined for classification: Bare/Built-up, Pasture, Forest, and Water. Bare/Built-up includes bare ground and built-up areas, such as bare soil, rock outcrops, sand, roads, infrastructure, urban areas, and other artificial surfaces. Pasture refers to grasslands used for cattle grazing or for fodder production (mowed meadows), including some agricultural fields; Forest comprises areas dominated by tree cover, including dry to humid forests, riparian forests, open to dense canopy, and high secondary vegetation; and Water includes rivers, streams, and stagnant water bodies.

The training data for the LC classification consisted of a shapefile with a total of 188 reference points (Figure 5), selected to represent stable LC classes across the study period. Each point was selected using PS and S2 true-colour (Red, Green, Blue) and false-colour (NIR, Red, Green) composites in QGIS (QGIS.org, 2025). Cloud- or shadow-affected pixels were excluded. Visual interpretation was further supported by historical high-resolution imagery from Google Earth (Google Earth, 2025). Additionally, field observations conducted in August 2024, guided by Prof. Carlos Devia (Pontificia Universidad Javeriana, 2025), provided contextual knowledge of forest and LC conditions in the study area. The distribution of reference points per class is presented in Table 1.

Table 1: Number of reference points per class used for land cover classification

Land Cover Class	**Number of Reference Points**
Bare/Built-up	53
Pasture	47
Forest	50
Water	38
Total	**188**

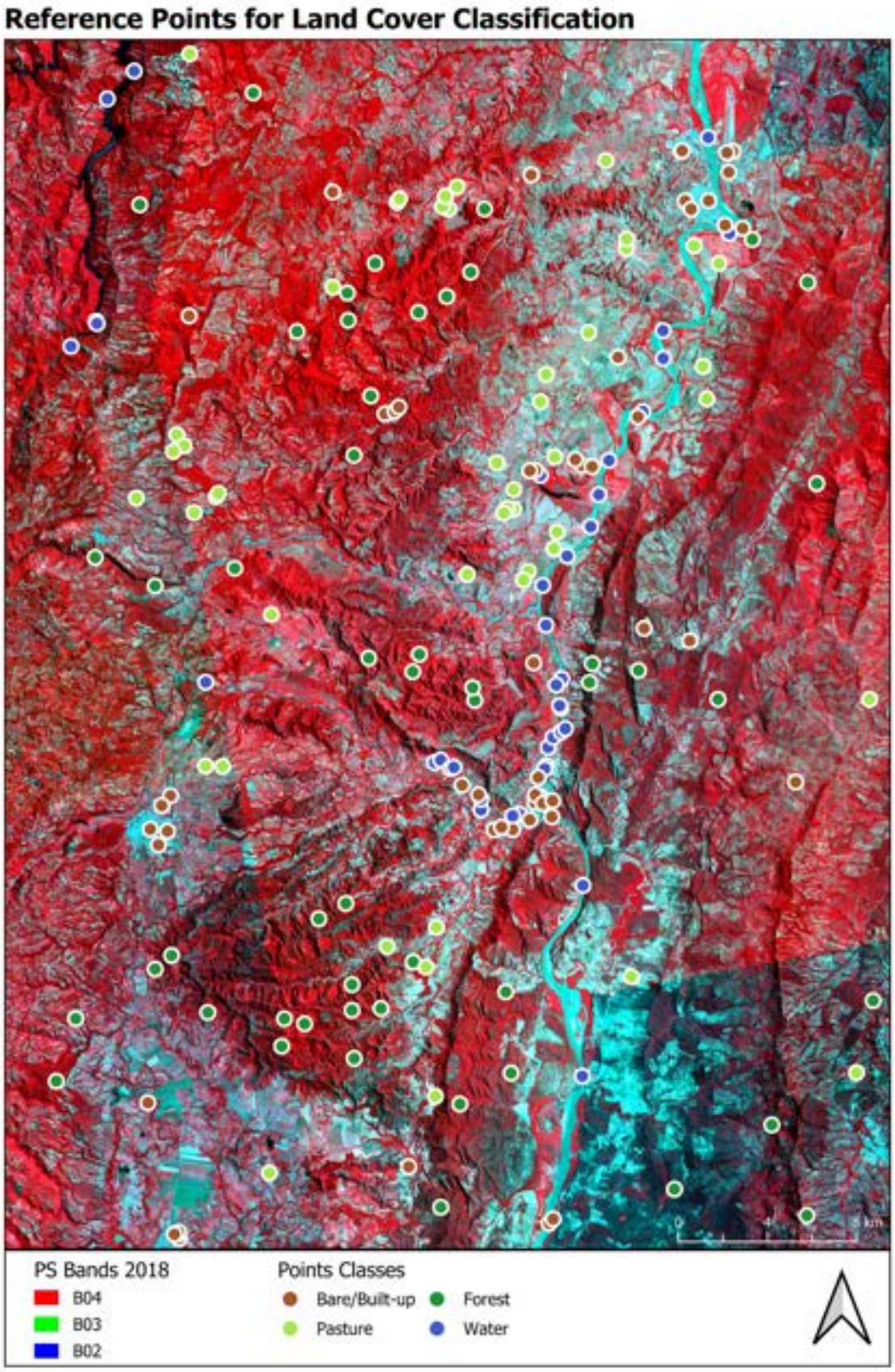


Figure 5: PlanetScope (PS) false-colour composite (NIR, Red, Green) from 2018 of the Area of Interest showing the reference points used for land cover classification. The four land cover classes are shown in brown (Bare/Built-up), light green (Pasture), dark green (Forest), and blue (Water).

2.3.2 Land Cover Classification using Random Forest Models

LC classification was performed to distinguish the four LC classes (Bare/Built-up, Pasture, Forest, and Water), as described above. A Random Forest (RF) classifier was used for this task. RF is a widely used machine learning algorithm that constructs multiple decision trees during the training process and merges their outputs to improve predictive performance and reduce overfitting (Breiman, 2001). As a non-parametric classifier, RF has been frequently used in LC mapping over the past decades (Gyamfi-Ampadu and Gebreslasie, 2021; Acharki, 2022; Ferrer Velasco *et al.*, 2022; Fagua and Jantz, 2024).

The RF model was run using default parameters: 500 trees for *ntree* (the number of trees grown in the ensemble) and the square root of the total number of input features for *mtry* (the number of variables considered at each split). Previous research has demonstrated that these default values yield adequate results (Liaw and Wiener, 2002; Pacheco-Pascagaza *et al.*, 2022).

Vegetation indices (VIs) (Table 2) were calculated in R using the *terra* package (R Core Team, 2021; Hijmans, 2025). For PS imagery (2018 – 2021), eight VIs (NDVI, SAVI, ARVI, RVI, GNDVI, IPVI, DD, EVI2) were derived from the four available spectral bands. For the period 2022 to 2024, PS imagery provided eight spectral bands, allowing the calculation of two additional red-edge-based indices (NDREI and RRI1). From S2 imagery, ten spectral bands and ten VIs (NDVI, SAVI, ARVI, RVI, GNDVI, NDREI, IPVI, DD, RRI1, EVI2) were derived.

The RF models were trained on multi-layer raster stacks combining spectral bands and VIs derived from PS and S2 datasets. Separate RF models were developed for each satellite dataset and year. In total, 14 RF models were generated to cover the years 2018 to 2024.

The RF models were implemented in R using the *randomForest* package (Liaw and Wiener, 2002; R Core Team, 2021). Accuracy was evaluated using confusion matrices computed with the *caret* package (Kuhn, 2008).

Table 2: Ten vegetation indices with names, abbreviations, and equations. PlanetScope (PS) and Sentinel-2 (S2) spectral band configurations used for index calculation are provided.

Index	Equation	Reference
Normalized Difference Vegetation Index	$NDVI = \frac{NIR - Red}{NIR + Red}$	(Rouse *et al.*, 1974)
Soil Adjusted Vegetation Index	$SAVI = \frac{1.5 \times (NIR - Red)}{NIR + Red + 0.5}$	(Huete, 1988)
Atmospherically Resistant Vegetation Index	$ARVI = \frac{NIR - (2 \times Red - Blue)}{NIR + (2 \times Red - Blue)}$	(Kaufman and Tanré, 1992)
Ratio Vegetation Index	$RVI = \frac{NIR}{Red}$	(Pearson and Miller, 1972; Jackson, Slater and Pinter, 1983)
Green Normalized Difference Vegetation Index	$GNDVI = \frac{NIR - Green}{NIR + Green}$	(Gitelson and Merzlyak, 1996)
Normalized Difference Red Edge Index	$NDREI = \frac{NIR - RedEdge}{NIR + RedEdge}$	(Gitelson, Kaufman and Merzlyak, 1996; Barnes *et al.*, 2000)
Infrared Percentage Vegetation Index	$IPVI = \frac{NIR}{NIR + Red}$	(Crippen, 1990)
Difference Difference Vegetation Index	$DD = (2 \times NIR - Red) - (Green - Blue)$	(Jackson, Slater and Pinter, 1983)
Red Edge Ratio Index 1	$RRI1 = \frac{NIR}{RedEdge}$	(Ehammer *et al.*, 2010)
Enhanced Vegetation Index 2	$EVI2 = \frac{2.5 \times (NIR - Red)}{NIR + (2.4 \times Red + 1)}$	(Jiang *et al.*, 2008)

PS (2018 – 2021): *Red:* B3, *Green:* B2, *Blue:* B1, *NIR:* B4

PS (2022 – 2024): *Red:* B5, *Green:* B3, *Blue:* B2, *NIR:* B8, *RedEdge:* B7

S2 (2018 – 2024): *Red:* B4, *Green:* B3, *Blue:* B2, *NIR:* B8, *RedEdge:* B5 (NDREI), B7 (RRI1)

2.3.3 Forest Cover Baseline Selection and Fragmentation Assessment

The baseline for forest loss assessment was derived from the PS LC classification map for 2018. PS imagery provides a spatial resolution of 3 m and has been used for LC mapping (Gašparović *et al.*, 2018; Acharki, 2022; Planet Labs PBC, 2025). The LC map was reclassified into a binary forest/non-forest map, where Forest = 1 and Non-forest = 0. The Non-forest category included the LC classes Bare/Built-up, Pasture, and Water.

To compare and cross-validate the 2018 Forest Cover Baseline, additional global and national forest cover datasets were consulted. The ESA WorldCover project provides global land cover products for 2020 and 2021, derived from Sentinel-1 and S2 data. It distinguishes 11 LC classes, including Tree cover, Shrubland, Grassland, Cropland, Built-up, Bare/sparse vegetation, Snow and ice, Permanent water bodies, Herbaceous wetland, Mangroves, and Moss and lichen (Zanaga *et al.*, 2021, 2022). The ESA WorldCover 2021 for the AOI is shown in Figure 6.

At the national scale, the IDEAM Corine LC (2018) product represents Colombia's LC, derived from Landsat imagery and adapted to the CORINE LLC methodology (IDEAM, 2010; IDEAM, PNN and Sinchi, 2021). The Figure 7 presents an adapted version for the area of interest, with grouped LC classes according to Table 3.

To characterise the 2018 Forest Cover Baseline and its forest fragmentation, 50 m and 100 m internal buffers were generated within all areas classified as forest. The 50 m buffer was used to represent forest edge conditions, while the 100 m buffer indicated forest core conditions. These distances were chosen because they fall within the commonly reported range of edge effects (~120 m), consistent with studies that apply similar buffers for edge-affected forest (Laurance *et al.*, 2002; Rodríguez, Balch and Rodríguez-Clark, 2007; Vancutsem *et al.*, 2021).

Table 3: Grouped land cover (LC) classes present in the area of interest. Codes (Código) and land cover classes (Cobertura) follow the national classification based on the CORINE Land Cover methodology adapted for Colombia (2018), developed by IDEAM, PNN and Sinchi (2021). English labels correspond to standard CORINE nomenclature, complemented with additional specific translations by ChatGPT (OpenAI, 2026).

LC Class	Código	Cobertura	CORINE + Specific English translation
Crops	2.1.2.1	Arroz	Rice fields
	2.1.2.2	Maíz	Non-irrigated arable land (maize)
	2.2.1.2.2	Caña panelera	Industrial crops (sugar cane for panela)
	2.2.3	Cultivos permanentes arbóreos	Permanent crops (tree crops)
Pasture	2.3.1	Pastos limpios	Pastures (managed/clean)
	2.3.2	Pastos arbolados	Pastures with scattered trees (wooded pastures)
	2.3.3	Pastos enmalezados	Pastures with natural vegetation encroachment (weedy pastures)
Mosaic	2.4.2	Mosaico de pastos y cultivos	Complex cultivation patterns (pastures and crops mosaic)
	2.4.3	Mosaico de cultivos, pastos y espacios naturales	Agriculture with significant natural vegetation (crops–pastures mosaic)
	2.4.4	Mosaico de pastos con espacios naturales	Pastures with natural vegetation (mosaic)

	2.4.5	Mosaico de cultivos con espacios naturales	Arable land with natural vegetation (crop mosaic)
Forest	3.1.1.1.1	Bosque denso alto de tierra firme	Broad-leaved forest (dense, terra firme, high)
	3.1.1.2.1	Bosque denso bajo de tierra firme	Broad-leaved forest (dense, terra firme, low)
	3.1.2.1.1	Bosque abierto alto de tierra firme	Transitional woodland-shrub (open forest, high)
	3.1.3.2	Bosque fragmentado con vegetación secundaria	Transitional woodland-shrub (fragmented forest)
	3.1.4	Bosque de galería y ripario	Riparian woodland (gallery forest)
	3.1.5	Plantación forestal	Forest plantations
Shrubs	3.2.1.1.1.1	Herbazal denso de tierra firme no arbolado	Natural grasslands (dense herbaceous, non-wooded)
	3.2.1.1.1.3	Herbazal denso de tierra firme con arbustos	Transitional woodland-shrub (herbaceous with shrubs)
	3.2.2.1	Arbustal denso	Sclerophyllous vegetation (dense shrubland)
	3.2.2.2	Arbustal abierto	Transitional woodland-shrub (open shrubland)
	3.2.3.1	Vegetación secundaria alta	Transitional woodland-shrub (tall secondary vegetation)
	3.2.3.2	Vegetación secundaria baja	Transitional woodland-shrub (low secondary vegetation)
Bare/ Built-up	1.1.1	Tejido urbano continuo	Continuous urban fabric
	1.1.2	Tejido urbano discontinuo	Discontinuous urban fabric
	1.2.1	Zonas industriales o comerciales	Industrial or commercial units
	1.2.2	Red vial, ferroviaria y terrenos asociados	Road and rail networks and associated land
	1.2.4	Aeropuertos	Airports
	3.3.1	Zonas arenosas naturales	Beaches, dunes, sands (natural sandy areas)
	3.3.3	Tierras desnudas y degradadas	Bare rocks / sparsely vegetated areas (degraded land)
Water	4.1.1	Zonas pantanosas	Inland marshes (swamps)
	5.1.1	Ríos (50 m)	Water courses (rivers, 50 m)
	5.1.2	Lagunas, lagos y ciénagas naturales	Water bodies (natural lakes, lagoons, wetlands)
	5.1.4	Cuerpos de agua artificiales	Water bodies (artificial)

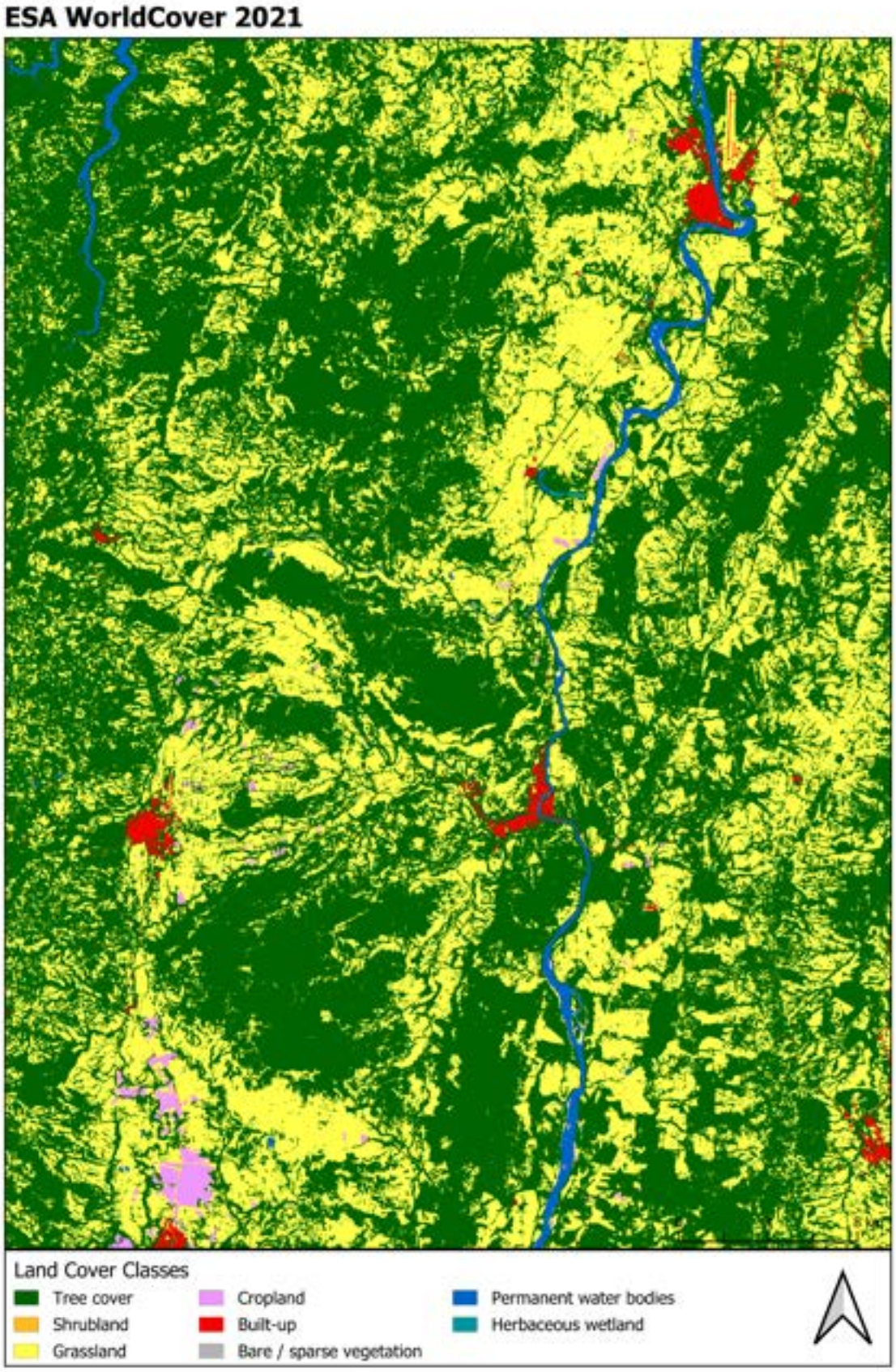


Figure 6: Land Cover map showing the area of interest in 2021 based on the ESA WorldCover project 2021. Contains modified Copernicus Sentinel data (2021) processed by ESA WorldCover consortium (Zanaga *et al.*, 2022).

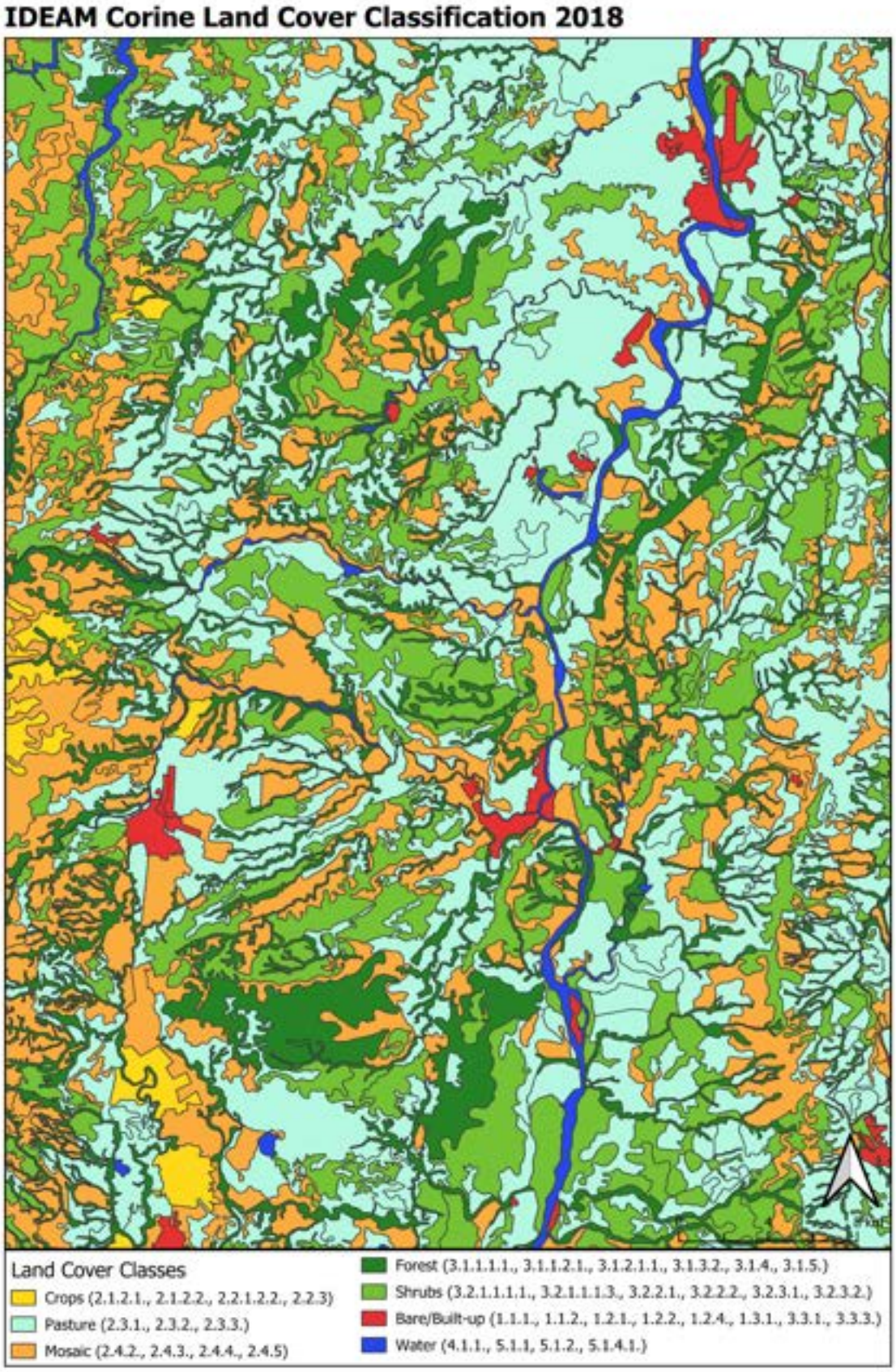


Figure 7: Land Cover map of the area of interest, derived from national CORINE Land Cover classification adapted for Colombia (2018), developed by IDEAM, PNN and Sinchi (2021). Land cover classes are grouped according to Table 3.

2.4 Forest Loss assessment

2.4.1 Change Detection based on Land Cover Classification

LC classifications were produced for each satellite dataset and each year, resulting in a total of 14 RF models covering the period 2018 – 2024. For every year, the classified raster was reclassified into a binary forest–non-forest map, where Forest = 1 and Non-forest = 0. The Non-forest category included the LC classes Bare/Built-up, Pasture, and Water.

Forest loss between two consecutive years was defined as a change from Forest in year t to any Non-forest class in year t + 1. Annual forest loss rasters (2019 – 2024) were generated accordingly and subsequently combined into a multi-year stack for each satellite dataset.

To ensure that only transitions from areas initially classified as forest were considered, masking with the 2018 Forest Cover Baseline was applied. This excluded all changes occurring in areas already classified as non-forest in the baseline year. The two resulting forest loss assessments were named: PS LC and S2 LC.

2.4.2 Change Detection based on Vegetation Index Thresholding using Reference areas

Reference areas for forest loss were identified by visually detecting patches of forest where tree cover was removed between consecutive years. Areas identified as forest in one year but showing little or no vegetation in the following year were considered as having experienced forest loss.

Each area was selected using PS and S2 true-colour (Red, Green, Blue) and false-colour (NIR, Red, Green) composites in QGIS (QGIS.org, 2025), by comparing imagery from one year with the next. Visual interpretation was supported by historical high-resolution imagery from Google Earth (Google Earth, 2025) and contextualized with field observations conducted in August 2024, guided by Prof. Carlos Devia (Pontificia Universidad Javeriana, 2025). Reference areas were further cross-checked with preliminary forest loss assessment results and the annual forest loss maps from the GFC product (Hansen *et al.*, 2013).

The spatial distribution of the reference areas is shown in Figure 8. Forest loss reference areas are indicated by circles, with colours corresponding to the year following the observed change. The number of reference areas per year ranges between 4 to 9 areas per year (Table 4), where sometimes a few smaller patches are marked within the same circle. An area containing many of the reference areas for forest loss was selected as zoom-in area (Figure 8). This area is located outside the three project areas. It was chosen to better illustrate local patterns of LC dynamics that may be less visible at the full-AOI scale. So instead of displaying maps of the entire AOI, a selected zoom-in area is shown for results on LC mapping and forest loss assessment.

Table 4: Number of reference areas for forest loss per year. The year indicates the year following the forest loss.

Year	2019	2020	2021	2022	2023	2024	**Total**
Number of reference areas	9	4	7	5	4	4	**33**



Figure 8: Sentinel-2 (S2) true-colour composite (Red, Green, Blue) from 2024 of the Area of Interest showing the reference areas for forest loss and the zoom-in area. The reference areas are indicated by circles, with colours corresponding to the year after the observed change.

In addition to change detection based on LC classification, a direct change detection approach using VIs was applied for forest loss assessment. Forest loss was identified using annual VI difference layers and threshold values. The workflow is illustrated in Figure 4.

A total of ten VIs were derived from PS and S2 imagery and used as input features for the RF model in the LC classification (Table 2). From the same set, three VIs were selected for further analysis in the VI difference layers: the Normalized Difference Vegetation Index (NDVI), the Soil Adjusted Vegetation Index (SAVI), and the Atmospherically Resistant Vegetation Index (ARVI). These indices were chosen due to their widespread use in vegetation monitoring and their sensitivity to canopy greenness, soil background effects, and atmospheric influences, respectively (Rouse *et al.*, 1974; Huete, 1988; Kaufman and Tanré, 1992).

Yearly difference layers were calculated for NDVI, SAVI, and ARVI from both PS and S2 imagery using:

$$Yearly\ Difference_{(t+1)} = Vegetation\ Index_{(t)} - Vegetation\ Index_{(t+1)}$$

Negative values indicate a reduction in vegetation greenness from one year to the next. Threshold values for forest loss were determined iteratively through visual inspection based on the reference areas (Figure 8). To maintain consistency, comparable thresholds were applied across the study area, throughout the time series, and between PS (Table 5) and S2 (

Table 6) datasets. Yearly difference layers were then reclassified into binary rasters, where forest loss (difference < threshold) was coded as 1 and no forest loss (difference ≥ threshold) as 0.

This procedure initially produced three forest loss assessments per satellite. For further comparison with other datasets, these were reduced to a single layer per satellite by combining SAVI and ARVI. NDVI, SAVI, and ARVI all respond similarly to vegetation cover (Rouse *et al.*, 1974; Huete, 1988; Kaufman and Tanré, 1992). However, SAVI accounts for soil influence, particularly relevant in dry forests with partial canopy and exposed soil, while ARVI mitigates atmospheric effects such as haze or non-uniform correction (Huete, 1988; Kaufman and Tanré, 1992). The SAVI+ARVI forest loss layer was created by multiplying the reclassified binary SAVI and ARVI layers, retaining only pixels that indicate forest loss in both indices. This approach reduces false detections caused by soil background or atmospheric variability.

Annual SAVI+ARVI forest loss layers were generated for each year, and a cumulative SAVI+ARVI forest loss raster was created by merging the six annual layers (2019 – 2024), representing total forest loss over the study period. To ensure that only genuine forest-to-non-forest transitions were included, a forest mask based on the 2018 Forest Cover Baseline was applied, excluding areas already classified as non-forest in 2018. The two resulting forest loss assessments were named: PS VIs and S2 VIs.

Table 5: Forest loss thresholds of yearly vegetation index differences for PlanetScope

PlanetScope		**Year**					
		2019	**2020**	**2021**	**2022**	**2023**	**2024**
Index	**NDVI**	-0.25	-0.25	-0.25	-0.25	-0.25	-0.25
	SAVI	-0.25	-0.25	-0.30	-0.25	-0.42	-0.25
	ARVI	-0.26	-0.26	-0.26	-0.26	-0.35	-0.26

Table 6: Forest loss thresholds of yearly vegetation index differences for Sentinel-2

Sentinel-2		Year					
		2019	**2020**	**2021**	**2022**	**2023**	**2024**
Index	**NDVI**	-0.25	-0.25	-0.32	-0.25	-0.25	-0.25
	SAVI	-0.35	-0.35	-0.35	-0.35	-0.35	-0.35
	ARVI	-0.26	-0.26	-0.32	-0.26	-0.32	-0.35

2.5 Global Forest Products

2.5.1 Hansen *et al.* Global Forest Change (GFC)

The GFC dataset provides a global overview of forest extent and change from 2000 to 2024, derived from Landsat imagery at 30 m spatial resolution (Hansen *et al.*, 2013). The data is freely available online for visualisation and further download under https://glad.earthengine.app/view/global-forest-change (GLAD, 2025). Hansen et al. (2013) characterized forest extent, loss, and gain from 2000 to 2012. In the study, trees are defined as vegetation taller than 5 m in height. Forest loss is defined as a stand-replacement disturbance. The Global Land Analysis and Discovery (GLAD) laboratory at the University of Maryland, in partnership with Global Forest Watch (GFW), updates forest loss data annually using a direct change detection approach. Annual forest loss is estimated using rules based on the maximum yearly decrease in percent tree cover and the maximum yearly decrease in the minimum growing season NDVI (Hansen *et al.*, 2013).

For this study, the "Year of gross forest cover loss event" layer was used, showing annual forest loss from 2000 to 2024. A subset covering 2018–2024 was created, including layers 2019 to 2024, where "2019" represents forest loss occurring between 2018 and 2019, and so on.

2.5.2 EC JRC Tropical Moist Forests (TMF)

The European Commission Joint Research Centre (EC JRC) provides the TMF product as part of their Tropical Forest Monitoring program. The TMF datasets are derived from Landsat imagery at 30 m spatial resolution, and the updated version (TMFv2024) is freely accessible online at https://forobs.jrc.ec.europa.eu/TMF/data (EC JRC, 2025). The product enables long-term monitoring of deforestation and forest degradation in the humid tropics from 1990 to 2024, covering the following Global Ecological Zones: tropical rain forest, tropical moist forest, tropical mountain systems, and tropical dry forest (Vancutsem *et al.*, 2021).

Vancutsem et al. (2021) developed an expert system that analyses Landsat imagery (1982 – 2019) to map TMF extent and forest change patterns. The system uses a sequential decision tree in which expert knowledge is encoded as rules. A disruption observation is recorded when a Landsat pixel shows a temporary loss of tree foliage on a single date. The total number of disruption observations provides an indication of disturbance intensity. Pixels with regrowing or remaining trees are classified as degraded forest, whereas deforestation is defined as a long-term conversion to non-forested land, visible for more than 2.5 years. Forest loss is determined by analysing the temporal sequence of these disruption observations (Vancutsem *et al.*, 2021). For this study, the "Deforestation year" layer was used to obtain annual forest loss data. A subset including layers 2019 to 2024 was created.

3. Results

3.1 Land Cover Maps

LC classification was performed to distinguish four LC classes (Bare/Built-up, Pasture, Forest, and Water) using a RF classifier. As detailed in the Methods section, the RF models were trained on multi-layer raster stacks combining spectral bands and VIs.

The performance of all 14 RF models, developed for each satellite dataset and year between 2018 and 2024, was evaluated using out-of-bag (OOB) estimates for overall accuracy (OA) and class-specific F1-scores. The results are presented in Table 7 for PS and Table 8 for S2. Across all models, the OA consistently exceeded 90%. The F1-scores ranged from 82.48% (PS 2022, Pasture class) to 100.00%, with eight instances achieving perfect F1-scores.

Table 7: Out-of-bag F1-scores per class and overall accuracy (OA) of Random Forest Models for PlanetScope by year

PlanetScope	**F1 Bare/Built-up**	**F1 Pasture**	**F1 Forest**	**F1 Water**	**OA**
2018	0.8679	0.8387	0.9505	0.9737	0.9043
2019	0.8598	0.8667	0.9703	0.9231	0.9043
2020	0.8846	0.8248	0.9505	0.9730	0.9043
2021	0.9715	0.9375	0.9697	1.0000	0.9681
2022	0.9245	0.9263	1.0000	0.9730	0.9574
2023	0.9333	0.9052	0.9800	1.0000	0.9468
2024	0.9039	0.8866	0.9800	0.9730	0.9362

Table 8: Out-of-bag F1-scores per class and overall accuracy (OA) of Random Forest Models for Sentinel-2 by year

Sentinel-2	**F1 Bare/Built-up**	**F1 Pasture**	**F1 Forest**	**F1 Water**	**OA**
2018	0.9423	0.8842	0.9505	1.0000	0.9415
2019	0.9346	0.8696	0.9307	1.0000	0.9309
2020	0.8932	0.8750	0.9608	0.9867	0.9255
2021	0.9615	0.9072	0.9495	1.0000	0.9521
2022	0.8824	0.8485	0.9293	0.9867	0.9043
2023	0.9333	0.8723	0.9505	1.0000	0.9362
2024	0.9231	0.8723	0.9608	1.0000	0.9362

The annual LC classifications for the years 2018 to 2024 are presented in Figure 9 for PS and Figure 10 for S2. These figures show the seven annual LC maps of the zoom-in area, along with a locator map indicating the position of the zoom-in area within the AOI. The zoom-in area enables detailed visual comparison that is not feasible at the full AOI scale.

The figures also include forest loss maps derived from changes between consecutive LC classifications, with colours indicating the year of change. Forest loss was defined as a transition from forest in year t to any non-forest class in year t+1.

Overall spatial patterns are similar between PS and S2 LC maps, although PS has a spatial resolution of 3 m compared to 10 m for S2.

The annual LC maps show transitions from forest to bare/built-up areas and, in some cases, water. These transitions correspond to those identified in the forest loss maps. In subsequent years, some of these areas are reclassified as pasture. Additional forest loss is observed along forest edges and in transition zones between forest and non-forest classes, where class boundaries are less stable across years.

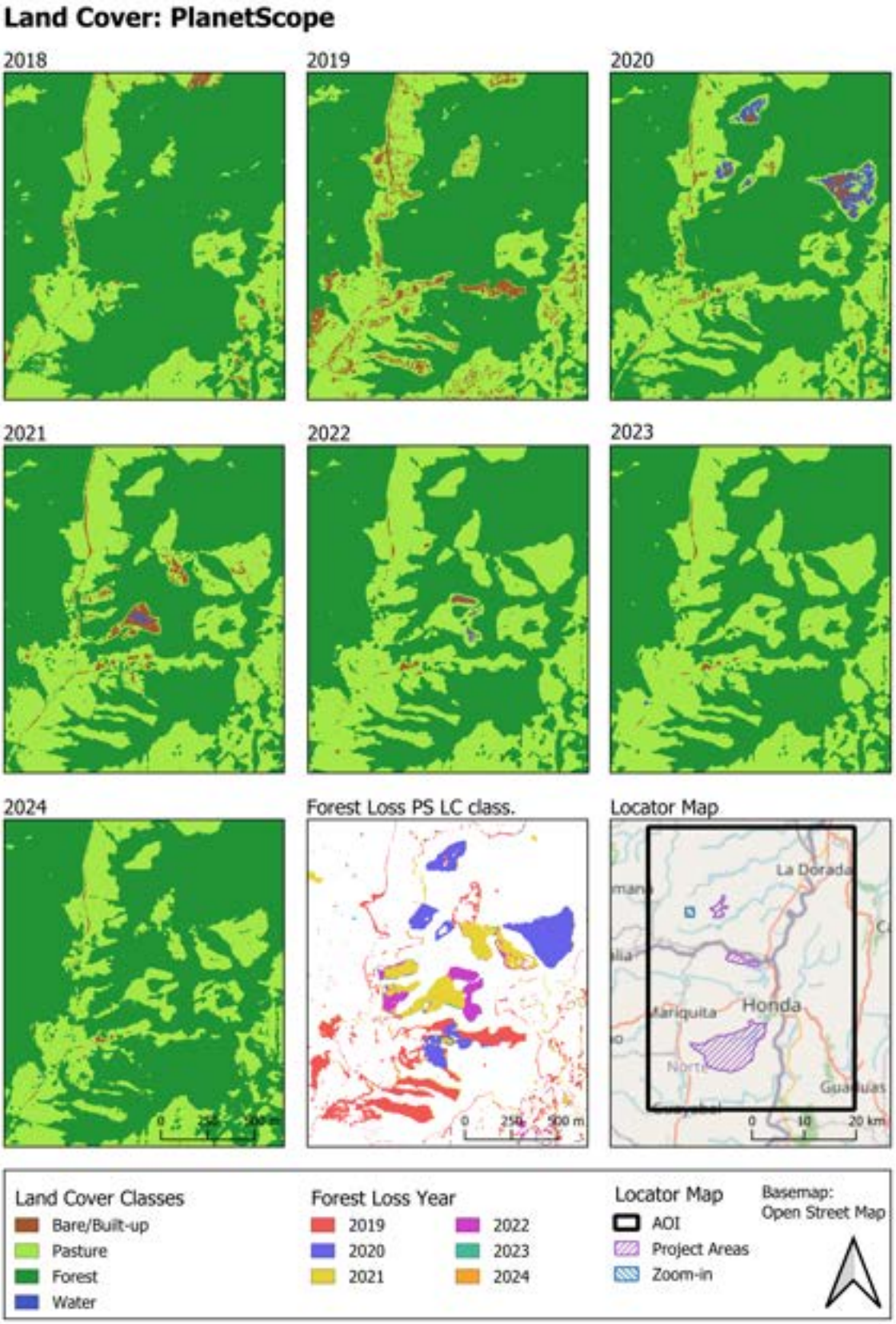


Figure 9: Annual land cover maps derived from PlanetScope imagery for 2018 – 2024, shown for the zoom-in area within the Area of Interest (AOI). The location of the zoom-in area is indicated in light blue on the locator map. Four land cover classes are distinguished: Bare/Built-up, Pasture, Forest, and Water. The forest loss map displays areas where "forest" transitioned to "Non-forest" between consecutive years, with colours indicating the year of forest loss (2019 – 2024).

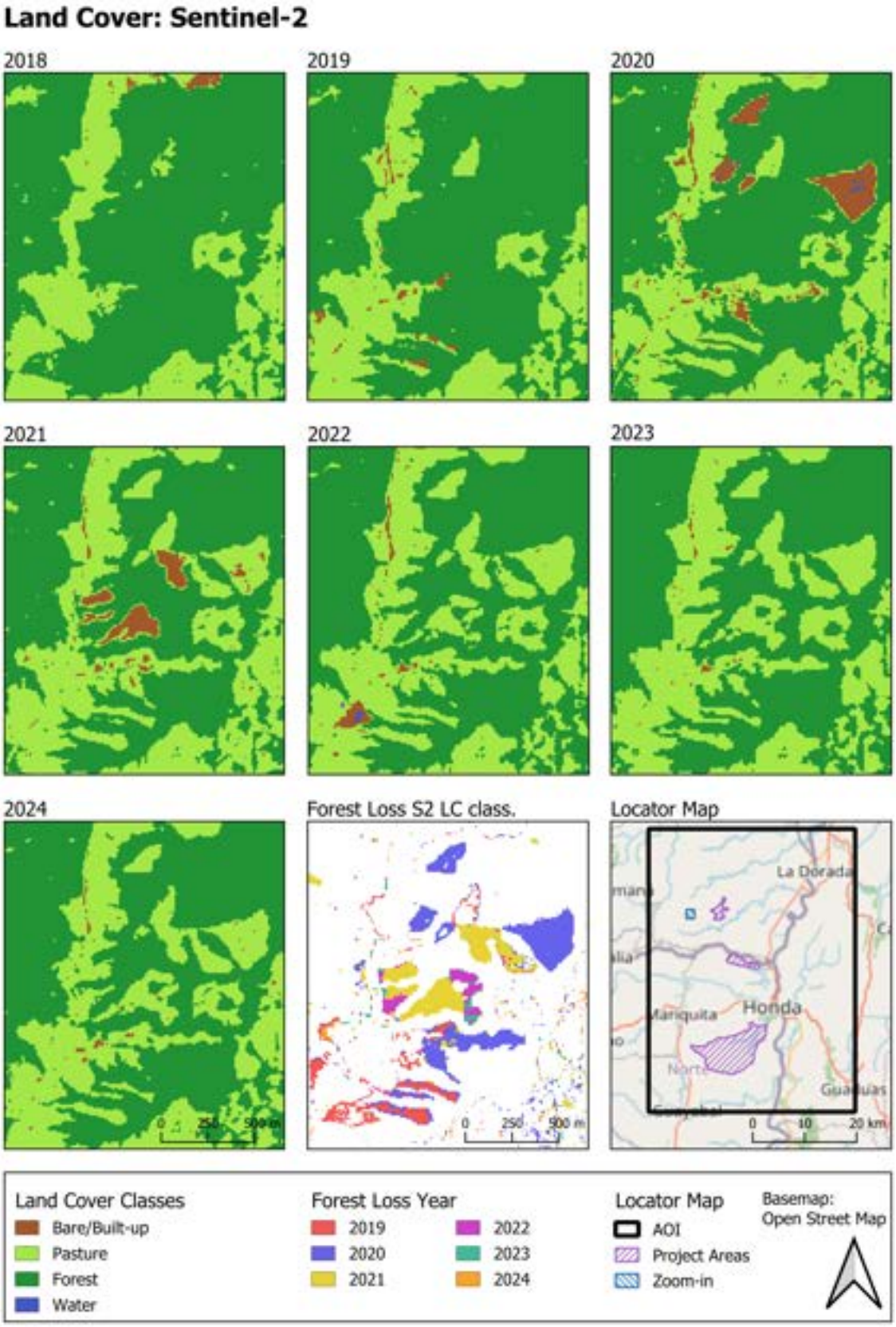


Figure 10: Annual land cover maps derived from Sentinel-2 imagery for 2018 – 2024, shown for the zoom-in area within the Area of Interest (AOI). The location of the zoom-in area is indicated in light blue on the locator map. Four land cover classes are distinguished: Bare/Built-up, Pasture, Forest, and Water. The forest loss map displays areas where "forest" transitioned to "Non-forest" between consecutive years, with colours indicating the year of forest loss (2019 – 2024).

3.2 Forest Cover Baseline

The forest cover baseline used for subsequent forest fragmentation and forest loss assessments is derived from the PS LC map for the year 2018. The original LC map was reclassified into a binary forest/non-forest dataset. The overall workflow of this process is illustrated in Figure 4.

The RF model applied to the PS 2018 dataset achieved a high overall accuracy (OA = 0.9043). The corresponding confusion matrix is presented in Table 9 and includes class-specific accuracy metrics. The F1-score for the forest class is 0.9505 (Table 7), which indicates a high level of classification accuracy for the forest/non-forest map.

Table 9: Confusion Matrix of Random Forest Model for PlanetScope 2018, including class-specific producer's accuracy (sensitivity), user's accuracy (positive predictive value) and overall accuracy (OA).

		Reference				Producer's Accuracy
		Bare/Built-up	Pasture	Forest	Water	
Prediction	Bare/Built-up	46	5	1	1	0.8679
	Pasture	6	39	1	0	0.8298
	Forest	0	3	48	0	0.9600
	Water	1	0	0	37	0.9737
User's Accuracy		0.8679	0.8478	0.9412	0.9737	OA = 0.9043

Forest cover distribution across the AOI, the zoom-in area and the three project areas is summarized in Table 10. Forest cover is highest in Las Mercedes (94.1%), followed by La Roka (68.0%) and El Triunfo (63.9%). At the AOI scale, forest and non-forest areas are nearly evenly distributed (49.8% forest, 50.2% non-forest), while the zoom-in area contains 72.3% forest.

Table 10: Forest and Non-Forest cover for the 3 project areas (Las Mercedes, La Roka and El Triunfo), the area of interest (AOI) and the zoom-in area in hectare and in percentage of the total area. Based on the 2018 Forest Cover Baseline.

Area	**Land Cover Class**	**Area** [ha]	**Percentage** [%]
Las Mercedes	Forest	503.3	94.1
	Non-forest	31.5	5.9
	Total	534.7	100.0
La Roka	Forest	502.7	68.0
	Non-forest	237.0	32.0
	Total	739.7	100.0
El Triunfo	Forest	4652.9	63.9
	Non-forest	2624.3	36.1
	Total	7277.3	100.0
AOI	Forest	107609.0	49.8
	Non-forest	108506.5	50.2
	Total	216115.5	100.0
Zoom-in	Forest	197.4	72.3
	Non-forest	75.5	27.7
	Total	273.0	100.0

Forest fragmentation was assessed using internal buffer distances of 50 m and 100 m from forest edges, as described in 2.3.3. Figure 11 shows the spatial distribution of forest edges and core areas within the AOI. Approximately 19.7% of the total forest area (21,242.5 ha) lies within 50 m of a forest edge, while 6.7% (7,175.5 ha) qualifies as core forest beyond 100 m from the edge (Table 11).

Table 11: Total forest cover of the area of interest (AOI) and the forest cover with minimum distance from edge 50 m and 100 m as areas in hectare and as percentage of the total forest cover. Based on the 2018 Forest Cover Baseline.

	Area [ha]	**Percentage** [%]
Total forest cover (AOI)	107609.0	100.0
Forest cover with minimum distance from edge: 50 m	21242.5	19.7
Forest cover with minimum distance from edge: 100 m	7175.5	6.7

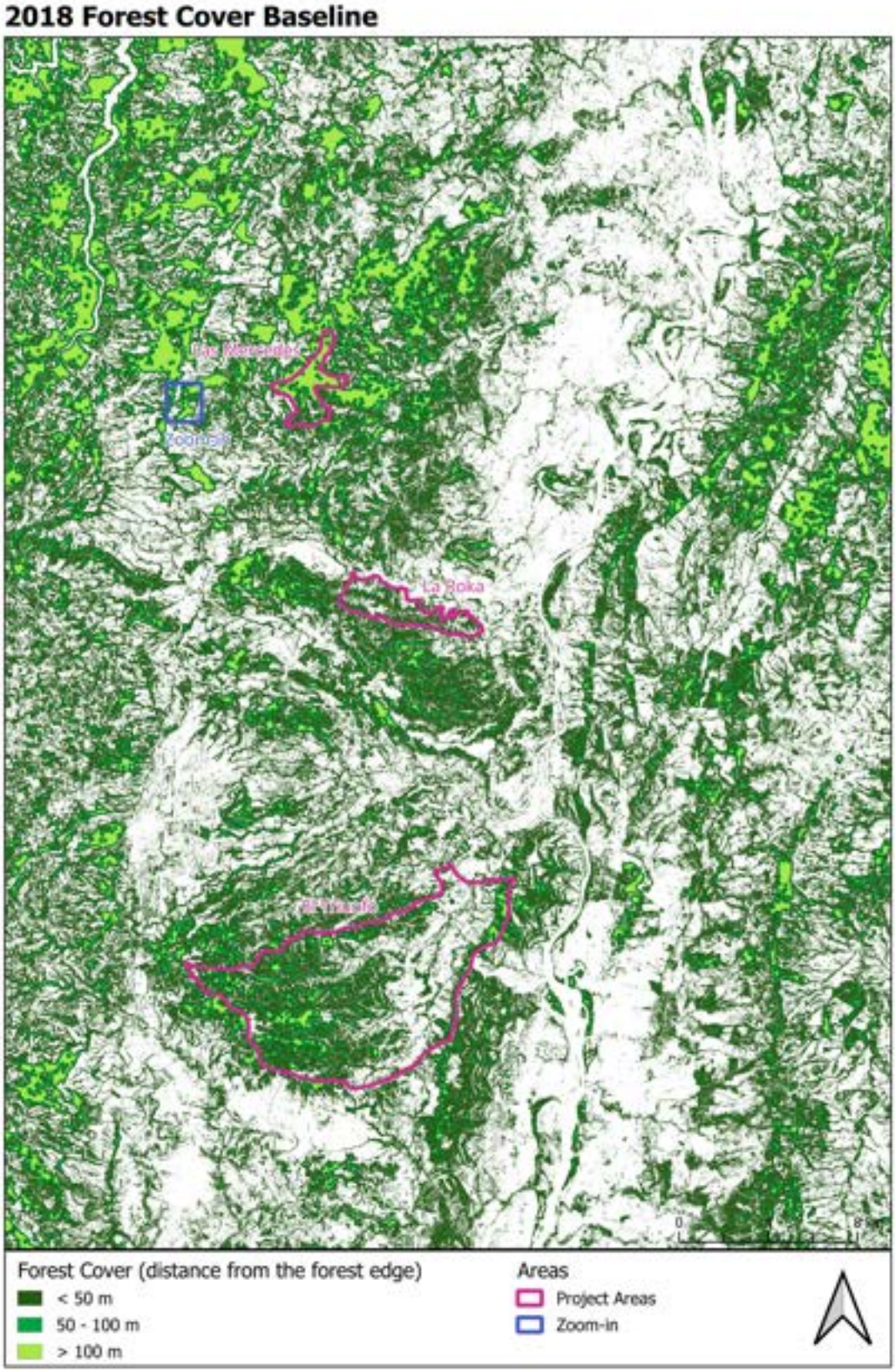


Figure 11: The 2018 Forest Cover Baseline of the area of interest showing forest cover and buffer zones used for fragmentation analysis. Forest cover is classified into three distance-based zones: < 50 m from the forest edge (dark green), 50 - 100 m from the edge (medium green), and > 100 m from the edge (light green). The three project areas (pink frame) and the zoom-in area (blue frame) are shown. The baseline is derived from the PlanetScope land cover classification for 2018.

3.3 Forest Loss

Forest loss between 2018 and 2024 was assessed using six datasets: PS VI, PS LC, S2 VI, S2 LC, GFC, and TMF. In all datasets, the term *Forest Loss Year* indicates the year in which forest cover change occurred (e.g., "2019" refers to forest loss between 2018 and 2019). The processing workflows leading to the forest loss outputs are summarized in Figure 4.

Spatial patterns across datasets are illustrated for the zoom-in area in Figure 12. The figure highlights differences in spatial resolution, with PS-based outputs (3 m) in the first row, S2-based outputs (10 m) in the second row, and Landsat-based products (30 m; GFC and TMF) in the third row. PS- and S2-based outputs show broadly similar spatial distributions of forest loss within the zoom-in area. In both cases, LC-based outputs (PS LC and S2 LC) detect larger forest loss areas than the corresponding VI-based outputs (PS VI and S2 VI). GFC overlaps with both VI and LC outputs in several locations, while TMF detects the smallest extent of forest loss, with limited spatial correspondence to the other datasets.

Forest loss patterns for the three project areas, Las Mercedes, La Roka, and El Triunfo, are shown in Figure 13, Figure 14 and Figure 15 respectively, using subareas. The location of each subarea is highlighted in green in the corresponding locator map. These subareas have the same spatial extent and scale as the zoom-in area presented in Figure 12, enabling visual comparison across datasets.

In Las Mercedes (Figure 13), minimal forest loss is observed across all datasets, with LC-based outputs capturing the largest extent. A small area of forest loss identified in 2021 shows agreement between GFC, VI-, and LC-based outputs. In La Roka (Figure 14), forest loss is limited in the VI-based outputs, GFC, and TMF, while LC-based outputs detect a greater extent of change. In El Triunfo (Figure 15), patterns are similar to those observed in the zoom-in area (Figure 12). GFC overlaps with both VI- and LC-based outputs in some locations, particularly for one area of forest loss in 2021. LC-based outputs show a larger extent of forest loss and capture changes occurring in multiple years.

Total forest loss from 2018 to 2024, expressed in hectares and as a percentage of the 2018 Forest Cover Baseline, is summarized in Table 12 for the AOI, the zoom-in area, and the three project areas. LC-based outputs (PS LC and S2 LC) report the highest loss, followed by VI-based outputs (PS VI and S2 VI) and GFC, with TMF showing the lowest values. Clear differences are evident among the project areas. Las Mercedes shows very low forest loss rates across all datasets (0.00 – 2.11%), La Roka exhibits higher and more variable forest loss rates (0.05 – 25.85%), and El Triunfo records the highest forest loss rates (0.14 – 35.30%).

Temporal patterns of forest loss are shown in Figure 16, which presents annual forest loss rates from 2019 to 2024 as a percentage of the 2018 Forest Cover Baseline for the AOI, the zoom-in area, and the three project areas. LC-based outputs consistently report higher annual forest loss than VI-based approaches and GFC across all spatial units. El Triunfo exhibits the highest annual forest loss, with a peak exceeding 800 ha in 2021 as detected by the S2 LC, while Las Mercedes shows consistently low annual forest loss values.

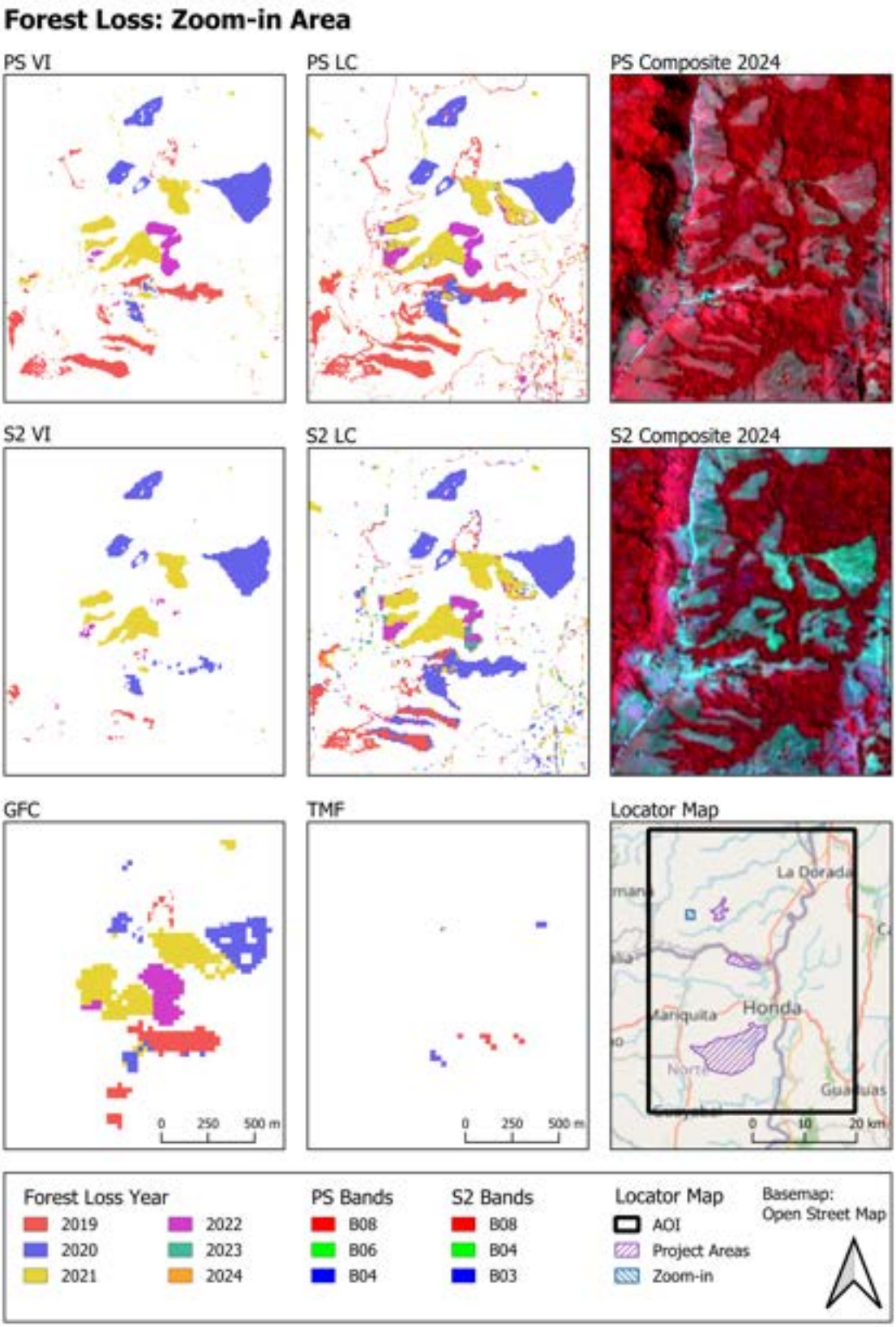


Figure 12: Forest loss maps for the zoom-in area, derived from six datasets: PS VI, PS LC, S2 VI, S2 LC, GFC, and TMF. Columns 1 and 2 show forest loss maps, with colours indicating the year of occurrence (2019 – 2024). Column 3 presents NIR false-colour composites of 2024 for PS and S2, along with the locator map. Abbreviations: PS = PlanetScope; S2 = Sentinel-2; VI = vegetation index; LC = land cover; GFC = Global Forest Change; TMF = Tropical Moist Forest.

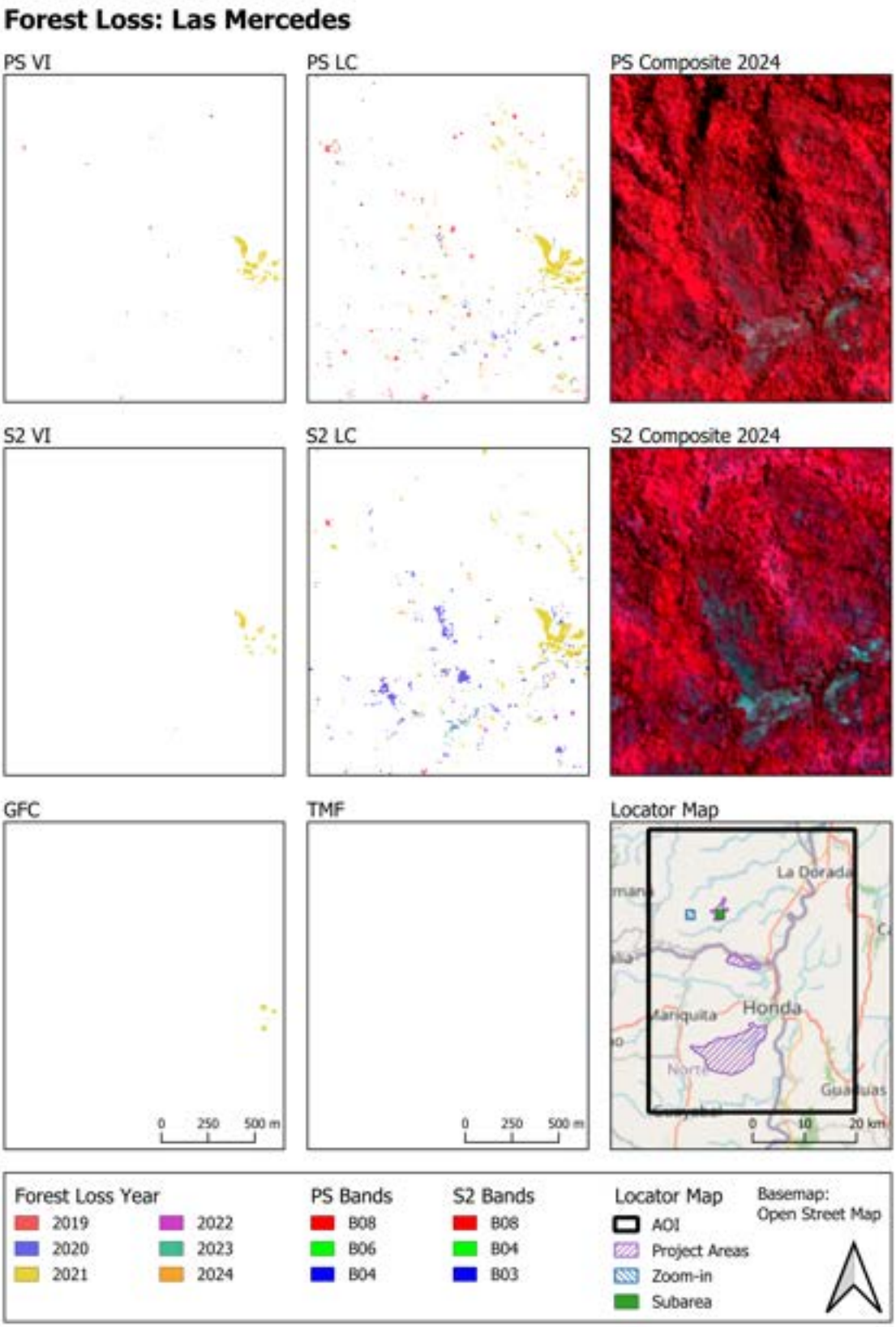


Figure 13: Forest loss maps for a selected subarea within of the project area "Las Mercedes", derived from six datasets: PS VI, PS LC, S2 VI, S2 LC, GFC, and TMF. Columns 1 and 2 show forest loss maps, with colours indicating the year of occurrence (2019 – 2024). Column 3 presents NIR false-colour composites of 2024 for PS and S2, along with the locator map. Abbreviations: PS = PlanetScope; S2 = Sentinel-2; VI = vegetation index; LC = land cover; GFC = Global Forest Change; TMF = Tropical Moist Forest.

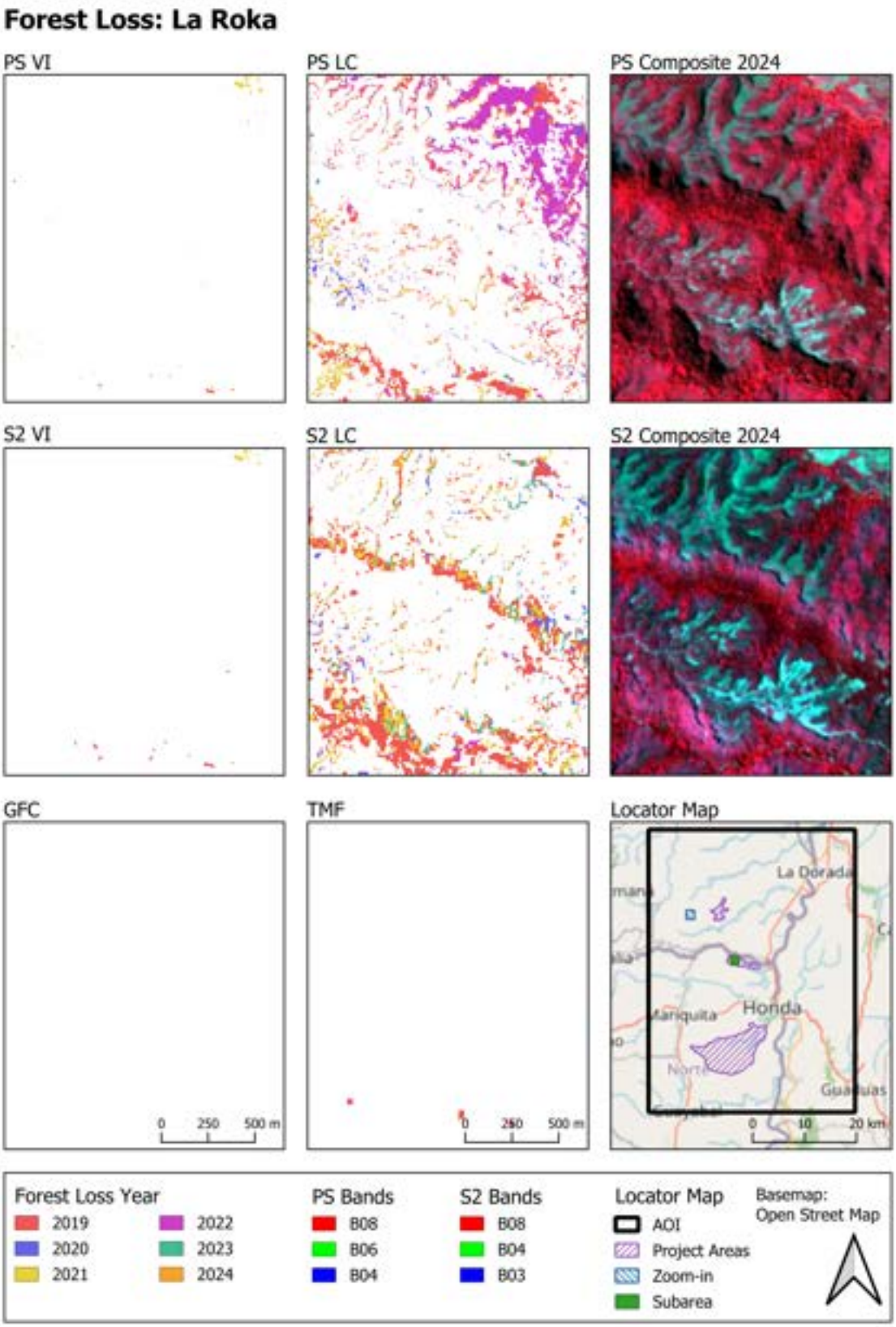


Figure 14: Forest loss maps for a selected subarea within of the project area “La Roka”, derived from six datasets: PS VI, PS LC, S2 VI, S2 LC, GFC, and TMF. Columns 1 and 2 show forest loss maps, with colours indicating the year of occurrence (2019 – 2024). Column 3 presents NIR false-colour composites of 2024 for PS and S2, along with the locator map. Abbreviations: PS = PlanetScope; S2 = Sentinel-2; VI = vegetation index; LC = land cover; GFC = Global Forest Change; TMF = Tropical Moist Forest.

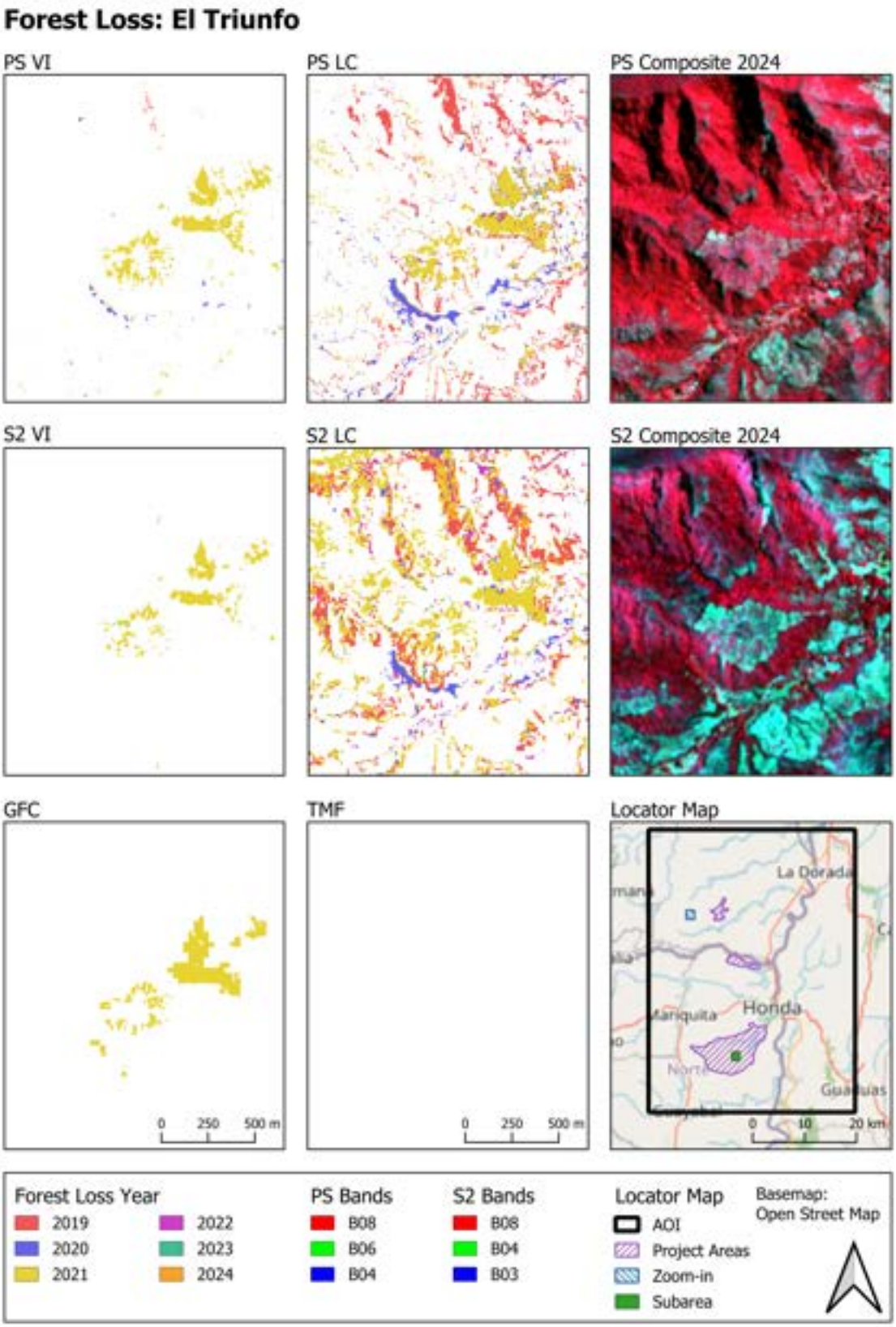


Figure 15: Forest loss maps for a selected subarea within of the project area "El Triunfo", derived from six datasets: PS VI, PS LC, S2 VI, S2 LC, GFC, and TMF. Columns 1 and 2 show forest loss maps, with colours indicating the year of occurrence (2019 – 2024). Column 3 presents NIR false-colour composites of 2024 for PS and S2, along with the locator map. Abbreviations: PS = PlanetScope; S2 = Sentinel-2; VI = vegetation index; LC = land cover; GFC = Global Forest Change; TMF = Tropical Moist Forest.

Table 12: Forest Loss totals (2018 – 2024) across the six datasets (PS VI, PS LC, S2 VI, S2 LC, GFC, and TMF) for the Area of Interest (AOI), Las Mercedes, La Roka, El Triunfo and the zoom-in area. The Forest Loss Rate (%) is calculated as the area of forest loss (ha) divided by the 2018 Forest Cover Baseline (ha).

Area	**Dataset**	**2018 Forest Cover Baseline** [ha]	**Forest Loss** [ha]	**Forest Loss Rate** [%]
AOI	PS VI	107609.0	5743.9	5.34
AOI	PS LC	107609.0	31165.2	28.96
AOI	S2 VI	107609.0	2779.3	2.58
AOI	S2 LC	107609.0	31663.8	29.42
AOI	GFC	107609.0	1976.3	1.84
AOI	TMF	107609.0	198.2	0.18
Las Mercedes	PS VI	503.3	0.6	0.12
Las Mercedes	PS LC	503.3	9.4	1.87
Las Mercedes	S2 VI	503.3	0.7	0.14
Las Mercedes	S2 LC	503.3	10.6	2.11
Las Mercedes	GFC	503.3	0.3	0.06
Las Mercedes	TMF	503.3	0.0	0.00
La Roka	PS VI	502.7	1.0	0.20
La Roka	PS LC	502.7	108.3	21.53
La Roka	S2 VI	502.7	0.3	0.05
La Roka	S2 LC	502.7	129.9	25.85
La Roka	GFC	502.7	1.1	0.22
La Roka	TMF	502.7	0.3	0.07
El Triunfo	PS VI	4652.9	70.7	1.52
El Triunfo	PS LC	4652.9	807.9	17.36
El Triunfo	S2 VI	4652.9	32.3	0.69
El Triunfo	S2 LC	4652.9	1642.7	35.30
El Triunfo	GFC	4652.9	38.5	0.83
El Triunfo	TMF	4652.9	6.3	0.13
Zoom-in	PS VI	197.4	31.0	15.68
Zoom-in	PS LC	197.4	51.9	26.27
Zoom-in	S2 VI	197.4	18.5	9.35
Zoom-in	S2 LC	197.4	48.2	24.42
Zoom-in	GFC	197.4	34.9	17.66
Zoom-in	TMF	197.4	1.2	0.59

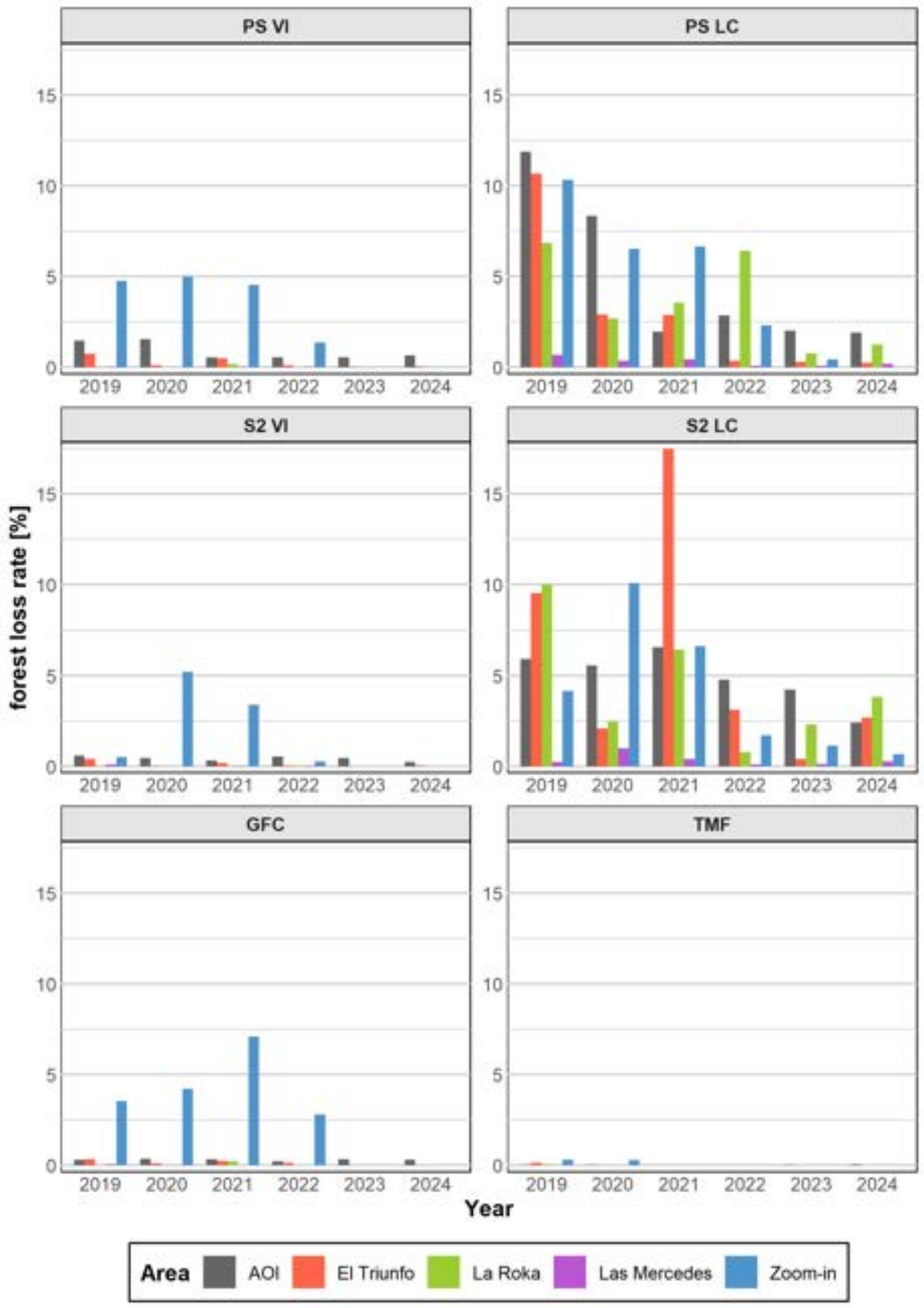


Figure 16: Annual forest loss rates (%) from 2019 to 2024 derived from six datasets: PS VI, PS LC, S2 VI, S2 LC, GFC, and TMF. Bars show forest loss rates for the Area of Interest (AOI), the zoom-in area, and the three project areas (Las Mercedes, La Roka, and El Triunfo), distinguished by colour. Abbreviations: PS = PlanetScope; S2 = Sentinel-2; VI = vegetation index; LC = land cover; GFC = Global Forest Change; TMF = Tropical Moist Forest.

4. Discussion

4.1 Evaluation of Land Cover Maps

The LC classifications derived from PS and S2 imagery form the basis for subsequent forest loss detection. Assessing their performance and potential sources of uncertainty is essential for interpreting the accuracy of the resulting maps and forest loss estimates.

PS and S2 provide satellite images with high resolution of 3 m and 10 m, respectively, and offer clear advantages for local and landscape-scale LC analyses (Acharki, 2022; Pacheco-Pascagaza *et al.*, 2022). Their fine spatial resolution enables the identification of narrow clearings, forest–pasture transitions, and small, fragmented forest remnants that are difficult to detect in moderate-resolution products (Pacheco-Pascagaza *et al.*, 2022; Fagua and Jantz, 2024). By reducing mixed-pixel effects, high-resolution imagery improves the representation of heterogeneous LC patterns typical of fragmented TDFs (Da Ponte *et al.*, 2015; Fremout *et al.*, 2022). The use of locally adapted reference areas further enhances classification performance by accounting for region-specific spectral and ecological characteristics (Pacheco-Pascagaza *et al.*, 2022; Fagua and Jantz, 2024).

Despite these strengths, several methodological constraints influenced classification reliability. Both the PS and S2 analyses relied on three-month mosaics (July to September) due to the limited availability of cloud-free imagery. In TDFs regions of the Colombian Andes, persistent cloud cover and complex topography strongly constrain image selection, making acquisition timing a critical factor for reliable change detection (De La Barreda-Bautista *et al.*, 2011; Prudente *et al.*, 2020). Optical remote sensing in these areas often requires seasonal or multi-date compositing to reduce data gaps (Da Ponte *et al.*, 2015; Prudente *et al.*, 2020; Pacheco-Pascagaza *et al.*, 2022; Pedraza *et al.*, 2024).

To produce the best mosaics under these constraints, scenes from July to September were selected each year to minimize seasonal variation and maximize cloud-free coverage. Fully cloud-free scenes were unavailable, so automated cloud-masking approaches, including the S2 Scene Classification Layer (SCL) (ESA, 2025) and composite generation in Google Earth Engine (Google Earth Engine, 2025), were tested but proved insufficient, leaving visible clouds and shadows. An alternative approach, not tested in this thesis, would be to use all available cloud-free pixels within a given year in a multi-temporal compositing framework. Another option would be to apply emerging satellite embedding methods, such as the Google DeepMind AlphaEarth Foundation (Brown *et al.*, 2025). Consequently, two to three partially cloud-covered scenes were manually processed per year in QGIS (QGIS.org, 2025): the largest and most suitable scene was used as the primary image, with clouded areas filled using additional scenes. Although minor cloud cover remained, this approach produced the most reliable mosaics feasible within available resources. Residual cloud and haze contamination may still affect spectral responses despite masking procedures, potentially introducing spurious change detections (Pacheco-Pascagaza *et al.*, 2022). In addition, temporal and spatial inconsistencies between composite images, as well as variations in illumination, solar geometry, and sensor characteristics, particularly within satellite constellations such as PS, can reduce comparability across years and lead to misclassifications (Acharki, 2022; Pedraza *et al.*, 2024; Daryaei *et al.*, 2025).

Classification accuracy metrics derived from PS (Table 7) and S2 (Table 8) indicate that both sensors provide a robust basis for forest monitoring. Overall accuracy exceeded 90% across all RF models, with F1-scores for the Forest class reaching approximately 0.97 for PS and 0.95 for S2. These results suggest that forest cover, the key class for subsequent loss detection, is mapped with high reliability. Classification uncertainty is not uniformly distributed across the landscape but is concentrated in

heterogeneous non-forest classes, particularly Pasture and Bare/Built-up, which exhibit greater internal variability and spectral overlap.

Validation of remote sensing classifications in tropical regions is frequently constrained by the absence of systematic ground reference data, which often necessitates a primary reliance on visual interpretation of very high-resolution imagery and cross-comparison with auxiliary datasets (Da Ponte *et al.*, 2015; Acharki, 2022; Fremout *et al.*, 2022; Pacheco-Pascagaza *et al.*, 2022). In this study, classification outputs were evaluated through contextual validation using field observations, expert knowledge, historical high-resolution imagery from Google Earth, and comparison with existing national and global LC datasets.

Field observations conducted in August 2024, together with expert guidance from Prof. Carlos Devia (Pontificia Universidad Javeriana, 2025), provided important contextual insight into local forest structure and land-use patterns that supported interpretation of the classification results. Historical imagery available through Google Earth further enabled visual verification of LC dynamics and the identification of reference areas used for VI-based forest loss thresholding.

Additional contextual comparison was conducted using national LC data by (IDEAM, PNN and Sinchi, 2021) (Figure 7) and the global ESA WorldCover dataset (Zanaga *et al.*, 2021) (Figure 6). While these products provide useful structural references for regional LC patterns, their relatively coarse mapping units and generalized classification schemes limit their suitability for validating local LC maps. In particular, the IDEAM dataset includes heterogenous “mosaic” classes, such as " Mosaico de pastos con espacios naturales / Mosaic of pastures with natural vegetation" (Table 3), that reflect the complex vegetation-agriculture landscapes typical in Colombia (Fernández-Méndez *et al.*, 2013; Pizano and García, 2014; IDEAM, PNN and Sinchi, 2021). These classes aggregate multiple LC types within a single unit, which complicates direct comparison with the LC classifications based on S2 or PS.

Consequently, validation relied on interpretation based on comparison with auxiliary datasets and field observations rather than independent *in situ* reference data. Despite these limitations, the broad spatial distribution of forest and agricultural LC in the produced maps corresponds well with patterns represented in the IDEAM and ESA datasets. This visual and structural alignment suggests a reasonable level of consistency with existing LC information (Figure 6, Figure 7).

4.2 Forest Cover Baseline Characterization

This section discusses the 2018 Forest Cover Baseline used for subsequent forest loss assessment. The 2018 LC classification derived from PS imagery was selected as the forest baseline due to its high spatial resolution (3 m), which enables detection of fine-scale forest patterns unresolved in coarser datasets based on Landsat imagery (Acharki, 2022; Fagua and Jantz, 2024; Daryaei *et al.*, 2025). This level of spatial detail is particularly important in heterogeneous TDF landscapes characterized by small forest remnants, narrow edge zones, and complex forest–pasture mosaics (Fernández-Méndez *et al.*, 2013; González-M *et al.*, 2018). Consistent with previous studies demonstrating improved LC discrimination using very high-resolution imagery, the PS-based classification provides a more spatially detailed representation of forest structure, capturing smaller tree patches and more precise boundaries than 10 m or 30 m sensors (Gašparović *et al.*, 2018; Daryaei *et al.*, 2025).

The 2018 Forest Cover Baseline analysis reveals a highly fragmented forest landscape (Figure 11). Forest cover is unevenly distributed across the three project areas, with Las Mercedes showing the highest proportion of forest cover, while La Roka and El Triunfo exhibit more heterogeneous forest–pasture mosaics. At the AOI level, forest and non-forest areas are nearly balanced (Table 10).

Fragmentation analysis further demonstrates that forest structure in the study area is strongly dominated by edge environments. Approximately 19.7% of forest area lies within 50 m of an edge, while only 6.7% lies 100 m from an edge (Table 11). This is a metric consistent with pantropical findings where a significant portion of undisturbed forest is considered edge-affected (e.g., within 120 m of a disturbance) (Vancutsem *et al.*, 2021). Ecologically, high edge density is associated with increased disturbance exposure, favouring generalist species and producing structurally and spectrally heterogeneous vegetation (González-M *et al.*, 2018).

Such structural patterns are characteristic of TDF landscapes across Latin America, particularly in the inter-Andean Magdalena Valley, where remaining forests are often restricted to riparian zones and steep slopes within a dominant agricultural matrix (Fernández-Méndez *et al.*, 2013; González-M *et al.*, 2018; Hasnat and Hossain, 2020).

From a remote sensing perspective, this landscape structure has direct implications for forest loss detection. High edge density increases the prevalence of mixed pixels and gradual transitions between forest and non-forest LC, which reduces classification stability (Da Ponte *et al.*, 2015; Galiatsatos *et al.*, 2020; Fremout *et al.*, 2022). Fragmentation, therefore, acts as a structural source of uncertainty in forest monitoring. Additionally, the inability of coarser products to resolve small fragments or narrow clearings explains why global products often underestimate forest loss in smallholder landscapes or open forests compared to high-resolution local assessments (Harris *et al.*, 2018; Galiatsatos *et al.*, 2020; Ferrer Velasco *et al.*, 2022; Fagua and Jantz, 2024).

4.3 Comparison of Forest Loss Assessment Approaches

Different remote sensing approaches can produce different forest loss estimates, depending on how change is detected and how classification uncertainty propagates through the analysis. This section, therefore, compares the forest loss results derived from two methodological approaches in order to evaluate their consistency and identify potential sources of variation.

Forest loss assessment was done with the two following approaches: (1) change detection based on annual LC classifications, and (2) direct forest loss detection using VIs thresholds, derived from PS and S2 imagery. Both methods were constrained by the 2018 Forest Cover Baseline to include only genuine forest-to-non-forest transitions.

LC-based outputs consistently reported higher forest loss than VI-based outputs for both PS and S2 (Figure 16; Table 12). This difference largely reflects methodological factors, as post-classification approaches are known to yield a much larger change surface than direct comparison methods (De La Barreda-Bautista *et al.*, 2011). Although annual LC classification achieved high accuracy, post-classification comparison can propagate errors: misclassifications at forest edges and transition zones may align across years, multiplying in the final change map and leading to an overestimation of forest loss (De La Barreda-Bautista *et al.*, 2011; Da Ponte *et al.*, 2015; Harris *et al.*, 2018).

In contrast, the VI-based approach relies on direct change detection using forest loss thresholds derived from SAVI and ARVI yearly difference layers. This method produces a map of forest loss between images from consecutive years, thereby eliminating the intermediate step of generating independent LC maps and reducing cumulative error propagation typical of post-classification comparison (De La Barreda-Bautista *et al.*, 2011; Da Ponte *et al.*, 2015; Harris *et al.*, 2018; Pacheco-Pascagaza *et al.*, 2022).

The selection of SAVI and ARVI, rather than relying solely on the NDVI, was motivated by the ecological and spectral characteristics of TDF ecosystems. Although NDVI, SAVI, and ARVI all respond to vegetation greenness and canopy cover (Rouse *et al.*, 1974; Huete, 1988; Kaufman and Tanré, 1992), their performance differs in heterogeneous and seasonally variable landscapes. SAVI

is particularly suited for areas with low vegetation cover and semi-arid conditions (Finger *et al.*, 2025). By incorporating a soil adjustment factor, SAVI reduces background reflectance effects caused by partial canopy cover and exposed soils (Huete, 1988). In TDFs, which often feature open canopies, pixels frequently consist of a mix of woody vegetation, herbaceous vegetation, and bare soil (Fremout *et al.*, 2022). SAVI mitigates soil background influences in these heterogeneous areas (Fremout *et al.*, 2022; Finger *et al.*, 2025). ARVI was included to address atmospheric variability. Optical remote sensing in tropical regions is frequently affected by haze, aerosols, and residual atmospheric correction inconsistencies (De La Barreda-Bautista *et al.*, 2011; Ferrer Velasco *et al.*, 2022; Pacheco-Pascagaza *et al.*, 2022). ARVI is specifically designed to minimize these atmospheric effects (Kaufman and Tanré, 1992), thereby reducing the likelihood of change detection errors caused by variations in atmospheric conditions between image dates (Ferrer Velasco *et al.*, 2022; Pacheco-Pascagaza *et al.*, 2022).

Forest loss assessment based on PS imagery can potentially outperform S2 in detecting smaller patches of forest loss due to its higher spatial resolution (3 m vs. 10 m) (Acharki, 2022; Daryaei *et al.*, 2025). The finer spatial detail enables the identification of smaller forest patches, narrow clearings, and more precise forest–non-forest boundaries than sensors with coarser resolution (Rösch *et al.*, 2022; Daryaei *et al.*, 2025). However, PS imagery is more variable in quality because it operates as a constellation of multiple satellites rather than a single platform with uniform specifications (Daryaei *et al.*, 2025; Planet Labs PBC, 2025). Inconsistencies in acquisition timing, solar altitude angles, and sensor characteristics result in varying illumination conditions and differing lengths and intensities of shadows. These variations increase spectral noise and may lead to misclassifications in both LC mapping and VI change detection (Daryaei *et al.*, 2025). In contrast, S2 provides more standardized acquisition conditions, including consistent viewing geometry, radiometric calibration, and 5-day revisit intervals (Daryaei *et al.*, 2025; ESA, 2025). This spectral consistency can reduce temporal variability in classification outputs. Additionally, S2 includes red-edge and shortwave infrared bands that enhance the detection of vegetation compared to PS's more limited spectral configuration (Daryaei *et al.*, 2025).

Despite these sensor-specific differences, variations in forest loss estimates between PS and S2 are likely driven by data availability and mosaic composition. Both analyses relied on three-month mosaics (July to September) due to the limited availability of cloud-free imagery. In the Colombian Andes, persistent cloud cover and complex topography constrain image selection, making acquisition timing a critical factor for reliable change detection (De La Barreda-Bautista *et al.*, 2011; Prudente *et al.*, 2020). Although PS offers near-daily revisit potential, many scenes had to be excluded due to spectral distortions, such as colour inconsistencies or atmospheric artefacts, resulting in fewer usable images than theoretically available (Daryaei *et al.*, 2025). Consequently, differences between PS and S2 forest loss assessments are likely influenced and limited less by inherent sensor resolution and more by temporal inconsistencies within mosaics and constraints in selecting high-quality, cloud-free imagery.

Overall, the S2 VI approach provides the most suitable balance between consistency and reliability for monitoring forest loss in the project areas. Compared to LC-based methods, it reduces error propagation associated with post-classification comparison, while the standardized acquisition conditions and spectral configuration of S2 support more stable temporal comparisons. Therefore, S2 VI is the most robust method for detecting forest loss among the tested approaches.

4.4 Forest Loss across Project Areas

Following the evaluation of methodological approaches and sensor performance, the three project areas of the "Reserva Natural de las Aguas", Las Mercedes, La Roka, and El Triunfo (Figure 2), are compared with respect to topography, forest cover, and land use. Examining the forest loss patterns across the three project areas reveals strong contrasts linked to landscape structure.

Las Mercedes, located in the northern part of the study area, is characterized by relatively intact vegetation and comparatively moist climatic conditions. The landscape is dominated by continuous forest cover, with approximately 94.1% of the area classified as forest in the 2018 Forest Cover Baseline. Las Mercedes exhibited a very low forest loss rate of 0.14% (S2 VI) between 2018 and 2024, with similarly low levels detected across the other datasets. This limited change likely reflects the high proportion of intact forest and relatively low accessibility. In tropical landscapes, accessibility is a key determinant of deforestation patterns, as land conversion and agricultural expansion tend to concentrate near settlements, agricultural land, and transport routes (De La Barreda-Bautista *et al.*, 2011; Ferrer Velasco *et al.*, 2022). The study by De La Barreda-Bautista et al. (2011) found that most detected changes occurred in easily accessible locations, typically within 90 – 150 m of settlements, water bodies, or previously cultivated areas, indicating localized agricultural expansion. Elevation may further contribute to these patterns, as Las Mercedes lies at relatively high elevations around Loma de Yarumal (731 masl). Elevation often acts as a proxy for accessibility, since steeper or higher terrain can limit agricultural expansion and infrastructure development (Ferrer Velasco *et al.*, 2022). Consequently, TDF loss has been most severe in low-altitude valleys, where agricultural suitability is highest (Portillo-Quintero and Sánchez-Azofeifa, 2010; Fagua and Jantz, 2024).

La Roka is located south of Las Mercedes at elevations between 250 and 400 masl. The climate is comparatively dry, and remaining forest patches are mainly restricted to slopes, while hilltops are rocky and sandy with significant erosion, making them too dry to support forest. This pattern is typical for the inter-Andean Magdalena Valley, where remaining forest is largely confined to riparian zones and steep slopes, while flatter and more fertile areas have been converted to agriculture (Fernández-Méndez *et al.*, 2013). The S2 VI forest loss rate for La Roka is 0.05%, likely reflecting that much of the original forest has already been converted to pasture, in contrast to the more intact Las Mercedes area. In addition, La Roka shows greater variability in forest loss across datasets. This variability likely reflects the dominance of forest-pasture mosaics, which create numerous edges and mixed pixels that increase classification uncertainty in remote sensing analyses (Da Ponte *et al.*, 2015).

El Triunfo represents the largest project area (7,277 ha) and showed the highest detected forest loss both in total area and relative rate. The S2 VI forest loss rate is 0.69%. El Triunfo also shows considerable variability in forest loss detection across datasets. The landscape in El Triunfo is characterized by a wide elevation range (250 – 800 masl), with remaining forest fragments mainly restricted to riparian zones and steep slopes, while flatter and more fertile areas have largely been converted to pasture for cattle ranching (Figure 3), a pattern typical of the Upper Magdalena River Valley (Fernández-Méndez *et al.*, 2013). Similar to La Roka, this heterogeneous landscape structure creates numerous edges and mixed pixels, increasing classification uncertainty and contributing to higher forest loss detected in the LC-based approach. In addition, the assessment in El Triunfo was further complicated by high cloud cover, a major limitation for optical remote sensing in the Colombian Andes (Pedraza *et al.*, 2024).

4.5 Evaluation of Forest Loss Detection across Datasets: Comparison of Global Forest Products and Forest Loss Assessment

Global forest monitoring products and locally adapted high-resolution analyses differ in their suitability for detecting forest loss in fragmented TDF landscapes. In this thesis, the suitability of global datasets, namely GFC and the TMF product, was assessed by comparing their forest loss estimates with those derived from higher-resolution forest loss assessment based on LC classification and VI approaches applied to PS and S2 imagery. In total, six datasets were compared. Global forest datasets provide standardized and accessible information at large spatial scales. The

GFC dataset, in particular, is widely recognized as a transparent, globally consistent, and reasonably accurate tool for monitoring broad deforestation trends at a 30 m resolution (Hansen *et al.*, 2013; Harris *et al.*, 2018). Across REDD+ countries, it serves as an unbiased proxy for tropical deforestation and can be broken down into national and subnational change statistics (Harris *et al.*, 2018). In contrast, high-resolution satellite data offer greater sensitivity to local disturbance processes but require more intensive processing and interpretation. This thesis highlights how differences in spatial resolution, detection algorithms, and forest definitions influence both the magnitude and spatial pattern of detected forest loss.

All six datasets detected forest loss between 2018 and 2024 yet estimates varied in magnitude and spatial detail (Figure 12, Table 12). LC-based approaches using PS and S2 reported the highest forest loss, followed by VI-based approaches and the GFC product, while the TMF dataset detected the lowest extent of loss. These differences reflect methodological characteristics rather than contradictory evidence of forest dynamics. Moreover, temporal definitions differ across datasets: this thesis uses only scenes from July to September for interannual change detection, GFC is produced on a calendar-year basis, whereas TMF relies on single-date observations and classifies deforestation only after a persistent change lasting more than 2.5 years. Visual comparison of mapped outputs with true- and false-colour composites indicates that most major forest loss areas were identified by all datasets except TMF, which detected only a limited number of pixels and showed no clear spatial pattern.

Agreement between GFC and VI-based approaches is expected, as both rely on spectral change detection derived from vegetation greenness metrics (Hansen *et al.*, 2013). In contrast, LC-based outputs showed extensive forest loss along forest–pasture boundaries, a pattern consistent with error propagation in post-classification change detection, where misclassifications in individual years accumulate in the final change map (De La Barreda-Bautista *et al.*, 2011; Da Ponte *et al.*, 2015). An alternative approach to mitigate this issue would be to consider only persistent changes confirmed over multiple years (e.g., requiring detection in two or three consecutive years), similar to the approach proposed by Vancutsem *et al.* (2021). This represents a potential direction for future work.

Differences in spatial resolution strongly influenced detection outcomes. The 3 m PS and 10 m S2 datasets captured fine-scale disturbances typical of fragmented TDF landscapes, including narrow clearings and edge-related forest conversion (Pacheco-Pascagaza *et al.*, 2022). In contrast, the 30 m Landsat-based global products often aggregated heterogeneous LC transitions within single pixels, leading to mixed-pixel effects and the underestimation of small-scale disturbances (Da Ponte *et al.*, 2015; Galiatsatos *et al.*, 2020; Fremout *et al.*, 2022). This effect is particularly relevant in landscapes dominated by mosaics of forest, pasture, and secondary vegetation, where deforestation frequently occurs at patch edges (Fernández-Méndez *et al.*, 2013). Previous studies have similarly shown that coarse-resolution datasets tend to miss disturbances occurring within one pixel of mapped loss, indicating systematic underdetection of edge-related change (Harris *et al.*, 2018; Fagua and Jantz, 2024).

Local adaptation of classification models further contributed to differences in forest loss estimates. The PS and S2 analyses were calibrated using locally representative training data, allowing them to capture region-specific spectral characteristics and phenological patterns (Pacheco-Pascagaza *et al.*, 2022; Fagua and Jantz, 2024). In contrast, global products rely on globally calibrated algorithms and validation samples from multiple ecological regions (Hansen *et al.*, 2013; Vancutsem *et al.*, 2021). While this standardization enables comparability across large spatial scales, it limits sensitivity to locally specific forest dynamics (Harris *et al.*, 2018; Ferrer Velasco *et al.*, 2022). Locally trained systems have been shown to detect a higher number of small and gradual forest loss events than global datasets, particularly in heterogeneous and seasonally variable ecosystems like the Colombian TDF (Da Ponte *et al.*, 2015; Harris *et al.*, 2018).

Methodological definitions of forest and forest loss also shaped the dataset performance (De La Barreda-Bautista *et al.*, 2011; Ferrer Velasco *et al.*, 2022). The GFC dataset identifies forest loss

primarily through abrupt spectral change associated with stand-replacement disturbance and decreases in vegetation greenness based on NDVI, which explains its relatively strong agreement with VI-based approaches (Hansen *et al.*, 2013; Galiatsatos *et al.*, 2020). However, Landsat resolution constraints and globally applied tree-cover thresholds may reduce sensitivity in areas with low canopy density or small-scale disturbance (Harris *et al.*, 2018).

The TMF product applies a more conservative definition of deforestation, requiring canopy loss to persist for more than 2.5 years (900 days) before classification, while shorter-term disturbances are classified as degradation. This approach is based on long-term temporal trajectories and evidential reasoning, allowing the algorithm to distinguish permanent forest conversion from temporary changes such as agricultural cycles or seasonal vegetation dynamics. Additionally, multi-year baseline requirements further reduce the risk of misclassifying non-forest land uses as deforestation (Vancutsem *et al.*, 2021). TMF has been shown to detect substantially larger areas of short-term disturbance than GFC at the pantropical scale, classifying these as degraded forests (Vancutsem *et al.*, 2021), which makes it particularly suitable for detecting forest degradation. Accordingly, the TMF approach is well-suited to reduce false positives in dynamic environments, especially where pasture clearing or agricultural cycles may otherwise be misclassified as forest loss. Specific rules are applied to minimize confusion with agricultural dynamics, particularly to avoid misinterpretation of fallow cycles (Vancutsem *et al.*, 2021). However, the dataset is optimized for closed evergreen and semi-evergreen forests in the humid tropics. Although its spatial coverage includes Global Ecological Zones classified as tropical dry forest (TDF) as well as tropical moist deciduous (monsoon) forests with a distinct dry season, its methodological design is less suited to these systems (Vancutsem *et al.*, 2021). As a result, TMF substantially underestimated forest loss in the study area, indicating limited suitability for monitoring fragmented TDF landscapes. Its inclusion nevertheless provides valuable insight into how differing definitions of forest loss influence detection outcomes, particularly in ecosystems where distinguishing between temporary disturbance and permanent conversion is inherently challenging.

High-resolution satellite datasets demonstrated advantages for landscape-scale forest monitoring but also introduced specific sources of uncertainty. Their spatial detail enables the detection of localized disturbance processes that remain invisible in global products (Pacheco-Pascagaza *et al.*, 2022). However, reliance on monotemporal mosaics introduces potential seasonal bias, and both classification-based and VI-based approaches are sensitive to methodological choices. Post-classification comparison can accumulate classification errors across years, particularly at forest edges, leading to overestimation of forest loss (De La Barreda-Bautista *et al.*, 2011). VI-based detection reduces this error propagation but remains sensitive to threshold selection and natural fluctuations in vegetation greenness. In TDF landscapes, where secondary vegetation dynamics and temporary pasture clearing are common, abrupt spectral changes do not always correspond to permanent forest removal (Da Ponte *et al.*, 2015; Ferrer Velasco *et al.*, 2022; George-Chacón *et al.*, 2022).

Despite these methodological differences, the magnitude and spatial distribution of detected forest loss are consistent with known deforestation processes in Colombian TDFs (Fernández-Méndez *et al.*, 2013; González-M *et al.*, 2018). Forest loss predominantly occurred along forest–pasture boundaries and within heterogeneous agricultural mosaics, corresponding to the “Mosaico de pastos con espacios naturales / Mosaic of pastures with natural vegetation” LC class described in national IDEAM datasets (IDEAM, PNN and Sinchi, 2021) (Table 3). Landscape structure and fragmentation influence forest loss further, as seen across the project areas.

Overall, the results indicate that global forest monitoring products are effective for identifying broad deforestation patterns and ensuring comparability across regions, but they are limited in their capacity to detect fine-scale forest dynamics in fragmented TDF landscapes. High-resolution, locally adapted monitoring approaches provide more detailed and sensitive assessments of forest change but require greater methodological effort and careful interpretation.

The integration of Digital Elevation Models (DEMs) can further improve accuracy, as elevation often serves as a proxy for accessibility, a key driver of deforestation where forest loss is concentrated near settlements and transport routes (De La Barreda-Bautista *et al.*, 2011; Ferrer Velasco *et al.*, 2022). In addition, the use of Synthetic Aperture Radar (SAR) data, such as Sentinel-1, provides cloud-independent information on vegetation structure and biomass, which is particularly valuable in Andean regions with persistent cloud cover (Joshi *et al.*, 2016; Ferrer Velasco *et al.*, 2022; Fagua and Jantz, 2024; Pedraza *et al.*, 2024). An effective monitoring strategy, therefore, combines the standardization of global datasets with the sensitivity of locally calibrated high-resolution imagery and structural radar data (Harris *et al.*, 2018; Pedraza *et al.*, 2024).

4.6 Conclusion

This thesis assessed the suitability of global forest datasets, particularly the GFC and the TMF product, for monitoring forest cover and forest loss in fragmented TDFs of central Colombia, and compared them to high-resolution satellite-based assessments using PS (3 m) and S2 (10 m).

The evaluation of LC classifications derived from S2 and PS demonstrates that high-resolution, locally calibrated remote sensing products provide a reliable basis for monitoring forest cover and detecting forest loss in fragmented TDFs. PS's 3 m resolution enables identification of small forest remnants, narrow edge zones, and fine-scale disturbances that coarser datasets often miss, while S2 offers greater spatial and spectral consistency and additional vegetation-sensitive bands.

Among the six datasets compared in this thesis, the S2 VI approach provides the most suitable balance between consistency, reliability, and local adaptability for monitoring forest cover and forest loss in the project areas. A high-quality and accurate forest cover baseline is essential for robust change detection and is a key prerequisite for reliable forest loss assessment. Forest loss estimates differ depending on the methodological approach: post-classification LC comparison tends to overestimate loss along edges, whereas VI-based methods reduce error propagation while remaining sensitive to natural temporal variability. Across the three project areas, forest loss patterns are strongly driven by landscape structure, topography, and accessibility, with minimal loss in intact high-elevation areas and higher, more variable loss in fragmented lowland areas. Among the global datasets, GFC showed good agreement with VI-based estimates, whereas TMF substantially underestimated forest loss, indicating limited suitability for monitoring TDFs in Colombia.

Global datasets are valuable for monitoring broad-scale deforestation patterns and ensuring comparability across regions. Nevertheless, their limitations in detecting small-scale disturbances within fragmented and heterogeneous TDFs require careful regional validation. Rather than being used as standalone monitoring solutions, global products should be integrated with locally adapted, high-resolution analyses to better capture the complexity of landscape dynamics. Future monitoring of fragmented TDFs should build on S2 VI approaches, complemented by SAR data to improve robustness under persistent cloud cover, while using global products such as GFC as an additional resource.

References

Acharki, S. (2022) “PlanetScope contributions compared to Sentinel-2, and Landsat-8 for LULC mapping,” *Remote Sensing Applications: Society and Environment*, 27. Available at: https://doi.org/10.1016/j.rsase.2022.100774.

Armenteras, D. *et al.* (2011) “Understanding deforestation in montane and lowland forests of the Colombian Andes,” *Regional Environmental Change*, 11(3), pp. 693–705. Available at: https://doi.org/10.1007/s10113-010-0200-y.

Barnes, E.M. *et al.* (2000) “Coincident detection of crop water stress, nitrogen status and canopy density using ground based multispectral data,” *Proceedings of the fifth international conference on precision agriculture, Bloomington, MN, USA*.

BOKU Kompetenzstelle für Klimaneutralität (2026) *Waldschutz im kolumbianischen Regenwald / Dorada*. Available at: https://klimaneutralität.boku.ac.at/projects/waldschutz-in-kolumbianischem-regenwald/ (Accessed: April 18, 2026).

Breiman, L. (2001) “Random Forests,” *Machine Learning*, 45(1), pp. 5–32. Available at: https://doi.org/10.1023/A:1010933404324.

Brown, C.F. *et al.* (2025) “AlphaEarth Foundations: An embedding field model for accurate and efficient global mapping from sparse label data,” *arXiv* [Preprint], (arXiv:2507.22291). Available at: https://doi.org/https://doi.org/10.48550/arXiv.2507.22291.

Bullock, S.H., Mooney, H.A. and Medina, E. (1995) “Introduction,” in S.H. Bullock, H.A. Mooney, and E. Medina (eds.) *Seasonally Dry Tropical Forests*. Cambridge: Cambridge University Press, pp. 1–8. Available at: https://doi.org/DOI: 10.1017/CBO9780511753398.001.

Copernicus (2025) *Sentinel-2 | Copernicus Data Space Ecosystem*, *dataspace.copernicus.eu*. Available at: https://dataspace.copernicus.eu/data-collections/copernicus-sentinel-data/sentinel-2 (Accessed: October 31, 2025).

Crippen, R.E. (1990) “Calculating the vegetation index faster,” *Remote Sensing of Environment*, 34(1), pp. 71–73. Available at: https://doi.org/10.1016/0034-4257(90)90085-Z.

Daryaei, A. *et al.* (2025) “Sentinel-2 vs. PlanetScope: Comparison and combination for tree species classification in two central European forest ecosystems,” *Remote Sensing Applications: Society and Environment*, 38. Available at: https://doi.org/10.1016/j.rsase.2025.101617.

Dexter, K.G. *et al.* (2018) “Inserting Tropical Dry Forests Into the Discussion on Biome Transitions in the Tropics,” *Frontiers in Ecology and Evolution*, 6. Available at: https://doi.org/10.3389/fevo.2018.00104.

Dirzo, R. *et al.* (2011) *Seasonally Dry Tropical Forests: Ecology and Conservation*. 1st ed. Washington, DC: Island Press/Center for Resource Economics. Available at: https://doi.org/10.5822/978-1-61091-021-7.

DRYFLOR *et al.* (2016) “Plant diversity patterns in neotropical dry forests and their conservation implications,” *Science*, 353(6306), pp. 1383–1387. Available at: https://doi.org/10.1126/science.aaf5080.

EC JRC (2025) *Tropical Moist Forests product - Data Access*, *Tropical Forest Monitoring*. Available at: https://forobs.jrc.ec.europa.eu/TMF/data (Accessed: November 3, 2025).

Ehammer, A. *et al.* (2010) “Statistical derivation of fPAR and LAI for irrigated cotton and rice in arid Uzbekistan by combining multi-temporal RapidEye data and ground measurements,” in C.M.U. Neale and A. Maltese (eds.) *Proceedings Volume 7824, Remote Sensing for Agriculture, Ecosystems, and Hydrology XII*. SPIE, p. 782409. Available at: https://doi.org/10.1117/12.864796.

ESA (2025) *SentiWiki: Sentinel-2 , sentiwiki.copernicus.eu*. Available at: https://sentiwiki.copernicus.eu/web/sentinel-2 (Accessed: October 31, 2025).

Etter, A., McAlpine, C. and Possingham, H. (2008) "Historical patterns and drivers of landscape change in Colombia since 1500: A regionalized spatial approach," *Annals of the Association of American Geographers*, 98(1), pp. 2–23. Available at: https://doi.org/10.1080/00045600701733911.

Fagua, J.C. and Jantz, P. (2024) "Mapping Tropical Dry Forest Gradients in an Andean Region with High Environmental Variability," *Ecological Indicators*, 168, p. 112744. Available at: https://doi.org/10.1016/j.ecolind.2024.112744.

Fernández-Méndez, F. *et al.* (2013) "Status of Knowledge, Conservation, and Management of Tropical Dry Forest in the Magdalena River Valley, Colombia," in G.A. Sánchez-Azofeifa et al. (eds.) *Tropical Dry Forests in the Americas: Ecology, Conservation, and Management*, pp. 35–54. Available at: https://doi.org/10.1201/b15417-6.

Ferrer Velasco, R. *et al.* (2022) "Towards accurate mapping of forest in tropical landscapes: A comparison of datasets on how forest transition matters," *Remote Sensing of Environment*, 274. Available at: https://doi.org/10.1016/j.rse.2022.112997.

Finger, A.P. *et al.* (2025) "Comparison Between Traditional Forest Inventory and Remote Sensing with Random Forest for Estimating the Periodic Annual Increment in a Dry Tropical Forest," *Forests*, 16(6), p. 998. Available at: https://doi.org/10.3390/f16060998.

Fremout, T. *et al.* (2022) "Site-specific scaling of remote sensing-based estimates of woody cover and aboveground biomass for mapping long-term tropical dry forest degradation status," *Remote Sensing of Environment*, 276. Available at: https://doi.org/10.1016/j.rse.2022.113040.

Galiatsatos, N. *et al.* (2020) "An assessment of global forest change datasets for national forest monitoring and reporting," *Remote Sensing*, 12(11). Available at: https://doi.org/10.3390/rs12111790.

Gašparović, M. *et al.* (2018) "Fusion of sentinel-2 and planetscope imagery for vegetation detection and monitoring," *International Archives of the Photogrammetry, Remote Sensing and Spatial Information Sciences - ISPRS Archives*. International Society for Photogrammetry and Remote Sensing, pp. 155–160. Available at: https://doi.org/10.5194/isprs-archives-XLII-1-155-2018.

George-Chacón, S.P. *et al.* (2022) "Mapping the spatial distribution of stand age and aboveground biomass from Landsat time series analyses of forest cover loss in tropical dry forests," *Remote Sensing in Ecology and Conservation*, 8(3), pp. 347–361. Available at: https://doi.org/10.1002/rse2.247.

Gitelson, A.A., Kaufman, Y.J. and Merzlyak, M.N. (1996) "Use of a green channel in remote sensing of global vegetation from EOS- MODIS," *Remote Sensing of Environment*, 58(3), pp. 289–298. Available at: https://doi.org/10.1016/S0034-4257(96)00072-7.

Gitelson, A.A. and Merzlyak, M.N. (1996) "Signature analysis of leaf reflectance spectra: Algorithm development for remote sensing of chlorophyll," *Journal of Plant Physiology*, 148(3–4), pp. 494–500. Available at: https://doi.org/10.1016/S0176-1617(96)80284-7.

GLAD (2025) *Global Forest Change*, *Google Earth Engine App*. Available at: https://glad.earthengine.app/view/global-forest-change (Accessed: November 3, 2025).

González-M, R. *et al.* (2018) "Disentangling the environmental heterogeneity, floristic distinctiveness and current threats of tropical dry forests in Colombia," *Environmental Research Letters*, 13(4). Available at: https://doi.org/10.1088/1748-9326/aaad74.

Google (2026) "NotebookLM." Available at: https://notebooklm.google.com/ (Accessed: May 21, 2026).

Google Earth (2025) *Historical imagery on Google Earth*, *Google*. Available at: https://earth.google.com/web/ (Accessed: October 31, 2025).

Google Earth Engine (2025) *Google Earth Engine*, *earthengine.google.com*. Available at: https://earthengine.google.com/ (Accessed: October 31, 2025).

Gregory-Wodzicki, K.M. (2000) "Uplift history of the Central and Northern Andes: a review," *Geological Society of America Bulletin*, 112(7), pp. 1091–1105. Available at: https://doi.org/https://doi.org/10.1130/0016-7606(2000)112<1091:UHOTCA>2.0.CO;2.

Gyamfi-Ampadu, E. and Gebreslasie, M. (2021) "Two decades progress on the application of remote sensing for monitoring tropical and sub-tropical natural forests: A review," *Forests*. MDPI AG. Available at: https://doi.org/10.3390/f12060739.

Hansen, M.C. *et al.* (2003) *Global Percent Tree Cover at a Spatial Resolution of 500 Meters: First Results of the MODIS Vegetation Continuous Fields Algorithm*, *Earth Interactions*. Available at: http://EarthInteractions.org.

Hansen, M.C. *et al.* (2013) "High-resolution global maps of 21st-century forest cover change," *Science*, 342(6160), pp. 850–853. Available at: https://doi.org/10.1126/science.1244693.

Harris, N. *et al.* (2018) *Comparing Global and National Approaches to Estimating Deforestation Rates in REDD+ Countries - Working Paper*. Washington, DC. Available at: https://www.wri.org/research/comparing-global-and-national-approaches-estimating-deforestation-rates-redd-countries (Accessed: October 30, 2025).

Hasnat, G.N.T. and Hossain, M.K. (2020) "Global Overview of Tropical Dry Forests," in R. Bhadouria et al. (eds.) *Handbook of Research on the Conservation and Restoration of Tropical Dry Forests*. Hershey, PA, USA: IGI Global Scientific Publishing, pp. 1–23. Available at: https://doi.org/10.4018/978-1-7998-0014-9.ch001.

Hesketh, M. and Sánchez-Azofeifa, A. (2014) "A review of remote sensing of tropical dry forests," *Tropical Dry Forests in the Americas. Ecology, Conservation, and Management Tropical Dry Forests*. Boca Raton: CRC Press, pp. 83–100.

Hijmans, R. (2025) "terra: Spatial Data Analysis." Available at: https://github.com/rspatial/terra (Accessed: October 31, 2025).

Huete, A.R. (1988) "A soil-adjusted vegetation index (SAVI)," *Remote Sensing of Environment*, 25(3), pp. 295–309. Available at: https://doi.org/10.1016/0034-4257(88)90106-X.

IDEAM (2010) *Leyenda Nacional de Coberturas de la Tierra: Metodología CORINE Land Cover Adaptada para Colombia. Escala 1:100.00*. Edited by N.J. Martínez Ardila and U.G. Murcia García. Bogotá, D.C., Colombia: Instituto de Hidrología, Meteorología y Estudios Ambientales.

IDEAM, PNN and Sinchi (2021) *Cobertura de la Tierra Metodología CORINE Land Cover Adaptada para Colombia Periodo 2018 a escala 1:100.000*. Bogotá D.C., Colombia.

Jackson, R.D., Slater, P.N. and Pinter, P.J. (1983) "Discrimination of growth and water stress in wheat by various vegetation indices through clear and turbid atmospheres," *Remote Sensing of Environment*, 13(3), pp. 187–208. Available at: https://doi.org/10.1016/0034-4257(83)90039-1.

Janzen, D. (1988) "Tropical dry forests: The most endangered major tropical ecosystem," in E.O. Wilson (ed.) *Biodiversity*. Washington (DC): National Academies Press (US), pp. 130–137.

Jiang, Z. *et al.* (2008) "Development of a two-band enhanced vegetation index without a blue band," *Remote Sensing of Environment*, 112(10), pp. 3833–3845. Available at: https://doi.org/10.1016/J.RSE.2008.06.006.

Joshi, N. *et al.* (2016) "A review of the application of optical and radar remote sensing data fusion to land use mapping and monitoring," *Remote Sensing*, 8(1). Available at: https://doi.org/10.3390/rs8010070.

Kaufman, Y.J. and Tanré, D. (1992) “Atmospherically Resistant Vegetation Index (ARVI) for EOS-MODIS,” *IEEE Transactions on Geoscience and Remote Sensing*, 30(2), pp. 261–270. Available at: https://doi.org/10.1109/36.134076.

Kuhn, M. (2008) “Building Predictive Models in R Using the caret Package,” *Journal of Statistical Software*, 28(5), pp. 1–26. Available at: https://doi.org/10.18637/jss.v028.i05.

De La Barreda-Bautista, B. *et al.* (2011) “Tropical Dry Forests in the Global Picture: The Challenge of Remote Sensing-Based Change Detection in Tropical Dry Environments,” in E. Carayannis (ed.) *Planet Earth 2011 - Global Warming Challenges and Opportunities for Policy and Practice*. London: IntechOpen. Available at: https://doi.org/10.5772/24283.

Laurance, W.F. *et al.* (2002) “Ecosystem Decay of Amazonian Forest Fragments: a 22-Year Investigation,” *Conservation Biology*, 16(3), pp. 605–618. Available at: https://doi.org/https://doi.org/10.1046/j.1523-1739.2002.01025.x.

Liaw, A. and Wiener, M. (2002) “Classification and regression by randomForest,” *R news*, 2(3), pp. 18–22. Available at: https://journal.r-project.org/articles/RN-2002-022/RN-2002-022.pdf.

Linares-Palomino, R., Oliveira-Filho, A.T. and Pennington, R.T. (2011) “Neotropical Seasonally Dry Forests: Diversity, Endemism, and Biogeography of Woody Plants,” *Seasonally Dry Tropical Forests*. Island Press/Center for Resource Economics, pp. 3–21. Available at: https://doi.org/10.5822/978-1-61091-021-7_1.

Miles, L. *et al.* (2006) “A global overview of the conservation status of tropical dry forests,” *Journal of Biogeography*, pp. 491–505. Available at: https://doi.org/10.1111/j.1365-2699.2005.01424.x.

Murphy, P.G. and Lugo, A.E. (1986) “ECOLOGY OF TROPICAL DRY FOREST,” *Annual Review of Ecology, Evolution, and Systematics*, 17(Volume 17), pp. 67–88. Available at: https://doi.org/https://doi.org/10.1146/annurev.es.17.110186.000435.

ÖIN (2026) *Las Mercedes Reserva Natural de las Agua*. Available at: https://oin.at/las-mercedes (Accessed: April 18, 2026).

Olson, D.M. *et al.* (2001) “Terrestrial Ecoregions of the World: A New Map of Life on Earth: A new global map of terrestrial ecoregions provides an innovative tool for conserving biodiversity,” *BioScience*, 51(11), pp. 933–938. Available at: https://doi.org/10.1641/0006-3568(2001)051[0933:TEOTWA]2.0.CO;2.

OpenAI (2026) “ChatGPT.” Available at: https://chat.openai.com (Accessed: May 21, 2026).

Pacheco-Pascagaza, A.M. *et al.* (2022) “Near Real-Time Change Detection System Using Sentinel-2 and Machine Learning: A Test for Mexican and Colombian Forests,” *Remote Sensing*, 14(3). Available at: https://doi.org/10.3390/rs14030707.

Pearson, R.L. and Miller, L.D. (1972) “Remote mapping of standing crop biomass for estimation of the productivity of the shortgrass prairie, Pawnee National Grasslands, Colorado.,” *Proceedings of the eighth international symposium on remote sensing of environment, October 2-6, 1972*. Ann Arbor, Michigan, USA: Willow Run Laboratories, Environmental Research Institute of Michigan, pp. 1357–1381.

Pedraza, C. *et al.* (2024) “Monitoring Forest Dynamics and Conducting Restoration Assessment Using Multi-Source Earth Observation Data in Northern Andes, Colombia,” *Forests*, 15(5). Available at: https://doi.org/10.3390/f15050754.

Pérez-Escobar, O.A. *et al.* (2022) “The Andes through time: evolution and distribution of Andean floras,” *Trends in Plant Science*. Elsevier Ltd, pp. 364–378. Available at: https://doi.org/10.1016/j.tplants.2021.09.010.

Pizano, C. and García, H. (2014) *El Bosque Seco Tropical en Colombia*. 1st ed. Edited by C. Pizano and H. García. Bogotá, D.C., Colombia: Instituto de Investigación de Recursos Biológicos Alexander von Humboldt (IAvH).

Planet Labs PBC (2025) *PlanetScope Product Specifications*. Available at: https://docs.planet.com/data/imagery/planetscope/ (Accessed: October 31, 2025).

Da Ponte, E. *et al.* (2015) "Tropical forest cover dynamics for Latin America using Earth observation data: a review covering the continental, regional, and local scale," *International Journal of Remote Sensing*, 36(12), pp. 3196–3242. Available at: https://doi.org/10.1080/01431161.2015.1058539.

Pontificia Universidad Javeriana (2025) *Carlos Alfonso Devia Castillo - Pontificia Universidad Javeriana, Perfiles y Capacidades de la Javeriana*. Available at: https://perfilesycapacidades.javeriana.edu.co/en/persons/cdevia/ (Accessed: October 31, 2025).

Portillo-Quintero, C.A. and Sánchez-Azofeifa, G.A. (2010) "Extent and conservation of tropical dry forests in the Americas," *Biological Conservation*, 143(1), pp. 144–155. Available at: https://doi.org/10.1016/j.biocon.2009.09.020.

Prudente, V.H.R. *et al.* (2020) "Limitations of cloud cover for optical remote sensing of agricultural areas across South America," *Remote Sensing Applications: Society and Environment*, 20. Available at: https://doi.org/10.1016/j.rsase.2020.100414.

QGIS.org (2025) "QGIS Geographic Information System." QGIS Association. Available at: https://doi.org/10.5281/zenodo.6139224.

R Core Team (2021) "R: A Language and Environment for Statistical Computing." Vienna, Austria: R Foundation for Statistical Computing. Available at: https://www.R-project.org/ (Accessed: October 31, 2025).

Rodríguez, J.P., Balch, J.K. and Rodríguez-Clark, K.M. (2007) "Assessing extinction risk in the absence of species-level data: Quantitative criteria for terrestrial ecosystems," *Biodiversity and Conservation*, 16(1), pp. 183–209. Available at: https://doi.org/10.1007/s10531-006-9102-1.

Rösch, M. *et al.* (2022) "Comparing PlanetScope and Sentinel-2 Imagery for Mapping Mountain Pines in the Sarntal Alps, Italy," *Remote Sensing*, 14(13). Available at: https://doi.org/10.3390/rs14133190.

Rouse, J.W. *et al.* (1974) "Monitoring vegetation systems in the great plains with ERTS," *Proceedings of the Third ERTS Symposium*. Washington, DC, USA: National Aeronautics and Space Administration, pp. 309–317.

Sánchez-Azofeifa, G.A. *et al.* (2013) "Tropical Dry Forests in the Americas: The Tropi-Dry Endeavor," *Tropical Dry Forests in the Americas*. CRC Press, pp. 19–34. Available at: https://doi.org/10.1201/b15417-4.

Vancutsem, C. *et al.* (2021) "Long-term (1990–2019) monitoring of forest cover changes in the humid tropics," *Science Advances*, 7(10), p. eabe1603. Available at: https://doi.org/10.1126/sciadv.abe1603.

Watson, J.E.M. *et al.* (2018) "The exceptional value of intact forest ecosystems," *Nature Ecology and Evolution*. Nature Publishing Group, pp. 599–610. Available at: https://doi.org/10.1038/s41559-018-0490-x.

Zanaga, D. *et al.* (2021) "ESA WorldCover 10 m 2020 v100," *ESA WorldCover* [Preprint]. Zenodo. Available at: https://doi.org/10.5281/zenodo.5571936.

Zanaga, D. *et al.* (2022) "ESA WorldCover 10 m 2021 v200," *ESA WorldCover* [Preprint]. Zenodo. Available at: https://doi.org/10.5281/zenodo.7254221.

Declaration of the use of generative AI tools

In the course of writing this master's thesis, I used generative AI tools, in particular ChatGPT (OpenAI, 2026) and NotebookLM (Google, 2026), as supporting tools.

AI tools assisted with programming and data analysis by helping to write, debug, and better understand R code. They were also used during the literature analysis, particularly for cross-checking references and linking selected sources to relevant text passages.

The writing process was also supported by AI tools. I used them to structure and plan the thesis and its sections, develop ideas for titles and headings, and transform bullet points or notes into coherent academic text. In addition, they were used to rephrase and refine passages, improve clarity and readability, and provide feedback on the overall structure and flow.

Furthermore, AI tools were used for translation purposes, including translating the abstract into German (Zusammenfassung) and supporting the translation and understanding of selected Spanish-language sources.

All outputs generated with the help of AI were carefully reviewed, adapted, and verified by me. The core ideas, analysis, and conclusions of this thesis are my own.

List of figures

Figure 1: Global distribution of tropical dry forest illustrating spatial variation in exposure to threats, including climate change, habitat fragmentation, fire, population density, and cropland conversion. The map shows tropical dry forest extent in 2000 based on biogeographic realms (Olson *et al.*, 2001) and MODIS 500 m forest cover data, with canopy cover > 40% (Hansen *et al.*, 2003). Robinson projection. Source: Miles et al. (2006). 8

Figure 2: Study Area in Central Colombia. Area of Interest (AOI) in red and the project areas of the "Reserva Natural de las Aguas" (Las Mercedes, La Roka, and El Triunfo) in purple. Cities are marked as brown points. 12

Figure 3: Pasture and forest patches in the project area El Triunfo, Colombia, August 2024. Image: author's own. 13

Figure 4: Flowchart illustrating the workflow of forest cover mapping and forest loss assessment. Rectangles represent data inputs and outputs, while rounded shapes indicate processing steps. Colours distinguish data types: red = input data, purple = auxiliary/reference data, blue = intermediate products, and green = final outputs. The workflow is divided into three components: forest cover mapping (grey background), forest loss assessment (blue dashed frame), and comparison with global forest products (red dashed frame). Abbreviations: PS = PlanetScope; S2 = Sentinel-2; VI = vegetation index; LC = land cover; GFC = Global Forest Change; TMF = Tropical Moist Forest. 16

Figure 5: PlanetScope (PS) false-colour composite (NIR, Red, Green) from 2018 of the Area of Interest showing the reference points used for land cover classification. The four land cover classes are shown in brown (Bare/Built-up), light green (Pasture), dark green (Forest), and blue (Water). 18

Figure 6: Land Cover map showing the area of interest in 2021 based on the ESA WorldCover project 2021. Contains modified Copernicus Sentinel data (2021) processed by ESA WorldCover consortium (Zanaga *et al.*, 2022). 23

Figure 7: Land Cover map of the area of interest, derived from national CORINE Land Cover classification adapted for Colombia (2018), developed by IDEAM, PNN and Sinchi (2021). Land cover classes are grouped according to Table 3. 24

Figure 8: Sentinel-2 (S2) true-colour composite (Red, Green, Blue) from 2024 of the Area of Interest showing the reference areas for forest loss and the zoom-in area. The reference areas are indicated by circles, with colours corresponding to the year after the observed change. 26

Figure 9: Annual land cover maps derived from PlanetScope imagery for 2018 – 2024, shown for the zoom-in area within the Area of Interest (AOI). The location of the zoom-in area is indicated in light blue on the locator map. Four land cover classes are distinguished: Bare/Built-up, Pasture, Forest, and Water. The forest loss map displays areas where "forest" transitioned to "Non-forest" between consecutive years, with colours indicating the year of forest loss (2019 – 2024). 31

Figure 10: Annual land cover maps derived from Sentinel-2 imagery for 2018 – 2024, shown for the zoom-in area within the Area of Interest (AOI). The location of the zoom-in area is indicated in light blue on the locator map. Four land cover classes are distinguished: Bare/Built-up, Pasture, Forest, and Water. The forest loss map displays areas where "forest" transitioned to "Non-forest" between consecutive years, with colours indicating the year of forest loss (2019 – 2024). 32

Figure 11: The 2018 Forest Cover Baseline of the area of interest showing forest cover and buffer zones used for fragmentation analysis. Forest cover is classified into three distance-based zones: < 50 m from the forest edge (dark green), 50 - 100 m from the edge (medium green), and > 100 m from the edge (light green). The three project areas (pink frame) and the zoom-in area (blue frame) are shown. The baseline is derived from the PlanetScope land cover classification for 2018. 35

Figure 12: Forest loss maps for the zoom-in area, derived from six datasets: PS VI, PS LC, S2 VI, S2 LC, GFC, and TMF. Columns 1 and 2 show forest loss maps, with colours indicating the year of occurrence (2019 – 2024). Column 3 presents NIR false-colour composites of 2024 for PS and S2, along with the locator map. Abbreviations: PS = PlanetScope; S2 = Sentinel-2; VI = vegetation index; LC = land cover; GFC = Global Forest Change; TMF = Tropical Moist Forest. 37

Figure 13: Forest loss maps for a selected subarea within of the project area “Las Mercedes”, derived from six datasets: PS VI, PS LC, S2 VI, S2 LC, GFC, and TMF. Columns 1 and 2 show forest loss maps, with colours indicating the year of occurrence (2019 – 2024). Column 3 presents NIR false-colour composites of 2024 for PS and S2, along with the locator map. Abbreviations: PS = PlanetScope; S2 = Sentinel-2; VI = vegetation index; LC = land cover; GFC = Global Forest Change; TMF = Tropical Moist Forest. 38

Figure 14: Forest loss maps for a selected subarea within of the project area “La Roka”, derived from six datasets: PS VI, PS LC, S2 VI, S2 LC, GFC, and TMF. Columns 1 and 2 show forest loss maps, with colours indicating the year of occurrence (2019 – 2024). Column 3 presents NIR false-colour composites of 2024 for PS and S2, along with the locator map. Abbreviations: PS = PlanetScope; S2 = Sentinel-2; VI = vegetation index; LC = land cover; GFC = Global Forest Change; TMF = Tropical Moist Forest. 39

Figure 15: Forest loss maps for a selected subarea within of the project area “El Triunfo”, derived from six datasets: PS VI, PS LC, S2 VI, S2 LC, GFC, and TMF. Columns 1 and 2 show forest loss maps, with colours indicating the year of occurrence (2019 – 2024). Column 3 presents NIR false-colour composites of 2024 for PS and S2, along with the locator map. Abbreviations: PS = PlanetScope; S2 = Sentinel-2; VI = vegetation index; LC = land cover; GFC = Global Forest Change; TMF = Tropical Moist Forest. 40

Figure 16: Annual forest loss rates (%) from 2019 to 2024 derived from six datasets: PS VI, PS LC, S2 VI, S2 LC, GFC, and TMF. Bars show forest loss rates for the Area of Interest (AOI), the zoom-in area, and the three project areas (Las Mercedes, La Roka, and El Triunfo), distinguished by colour. Abbreviations: PS = PlanetScope; S2 = Sentinel-2; VI = vegetation index; LC = land cover; GFC = Global Forest Change; TMF = Tropical Moist Forest. 42

List of tables

Table 1: Number of reference points per class used for land cover classification 17

Table 2: Ten vegetation indices with names, abbreviations, and equations. PlanetScope (PS) and Sentinel-2 (S2) spectral band configurations used for index calculation are provided. 20

Table 3: Grouped land cover (LC) classes present in the area of interest. Codes (Código) and land cover classes (Cobertura) follow the national classification based on the CORINE Land Cover methodology adapted for Colombia (2018), developed by IDEAM, PNN and Sinchi (2021). English labels correspond to standard CORINE nomenclature, complemented with additional specific translations by ChatGPT (OpenAI, 2026). 21

Table 4: Number of reference areas for forest loss per year. The year indicates the year following the forest loss. 25

Table 5: Forest loss thresholds of yearly vegetation index differences for PlanetScope 27

Table 6: Forest loss thresholds of yearly vegetation index differences for Sentinel-2 28

Table 7: Out-of-bag F1-scores per class and overall accuracy (OA) of Random Forest Models for PlanetScope by year 29

Table 8: Out-of-bag F1-scores per class and overall accuracy (OA) of Random Forest Models for Sentinel-2 by year 29

Table 9: Confusion Matrix of Random Forest Model for PlanetScope 2018, including class-specific producer's accuracy (sensitivity), user's accuracy (positive predictive value) and overall accuracy (OA). 33

Table 10: Forest and Non-Forest cover for the 3 project areas (Las Mercedes, La Roka and El Triunfo), the area of interest (AOI) and the zoom-in area in hectare and in percentage of the total area. Based on the 2018 Forest Cover Baseline. 34

Table 11: Total forest cover of the area of interest (AOI) and the forest cover with minimum distance from edge 50 m and 100 m as areas in hectare and as percentage of the total forest cover. Based on the 2018 Forest Cover Baseline. 34

Table 12: Forest Loss totals (2018 – 2024) across the six datasets (PS VI, PS LC, S2 VI, S2 LC, GFC, and TMF) for the Area of Interest (AOI), Las Mercedes, La Roka, El Triunfo and the zoom-in area. The Forest Loss Rate (%) is calculated as the area of forest loss (ha) divided by the 2018 Forest Cover Baseline (ha). 41